AN EXPERIMENTAL INVESTIGATION OF IONIZATION OF SUPERSONIC AIR BY A CORONA DISCHARGE

By

UDYAVAR S. SATYANAND

Presented to the Faculty of the Graduate School of

The University of Texas at Arlington in Partial Fulfillment

of the Requirements

for the Degree of

DOCTOR OF PHILOSOPHY

THE UNIVERSITY OF TEXAS AT ARLINGTON

August 2005

DEDICATION

This dissertation is dedicated to my wife, S. B. Nagamani, my daughter, Jyothi Kiran, and my son, Jai Kishan for their unflinching support and encouragement all the way through my PhD program at UTA, Arlington, Tx, USA.

ACKNOWLEDGEMENTS

I wish to thank the members of my committee for their assistance in completing this work.

It was a great privilege for me to work under my supervisor, Dr. Frank K. Lu. I thank him for exhibiting confidence in my ability and for the encouragement to work on this project. His expertise in experimental studies profoundly benefited me in successfully completing this work.

I also feel very proud to be guided by my supervisor, Dr. George Emanuel. His constant motivation and relentless monitoring of the progress throughout this work helped me to achieve success. I was greatly benefited by his sound background of aerodynamics. I am indebted to him for all the help I received.

I also wish to thank Dr. Bernard T. Svihel, Professor, Electrical and Electronics Engineering Department, UTA, for the continuous involvement, encouragement and material support during this work.

I owe my sincere gratitude to Dr. Frank K. Lu, Dr. George Emanuel, and Dr. Bernard T. Svihel for the financial support extended to carry out this project.

I wish to thank Dr. Donald R. Wilson, Professor, Mechanical and Aerospace Engineering Department, who was always receptive to my queries.

I would like to thank Prof. Feng C. Lai, School of Aerospace and Mechanical Engineering, University of Oklahoma, for useful discussions.

I wish to thank Philip K. Panicker, graduate student, but for whose active support, I would not have completed this work. He built all the electrical equipment used in this work.

My sincere thanks are also due to Rod Duke, technician, Aerodynamics Research Center, whose help in this project is really commendable. His technical support, both theoretical and practical, was enormous.

I would like to thank Dr. Wei-Jen Lee, Professor, Electrical Engineering Department, UTA, for his help in plasma detection. I also thank Rusty Wayne for the technical support in building amplifiers for this project.

Finally I thank all my colleagues at Aerodynamics Research Center, UTA, who helped me during this project.

ABSTRACT

AN EXPERIMENTAL INVESTIGATION OF IONIZATION OF

SUPERSONIC AIR BY A CORONA DISCHARGE

Publication No. _____

Udyavar S. Satyanand, Ph.D.

The University of Texas at Arlington, 2005

Supervising Professors: Frank K. Lu, George Emanuel.

A technique is developed to ionize supersonic air flow in a shock tube by a weak corona discharge. The driven section of the tube is open to the atmosphere. The shock propagates in the driven section at about 1 km/s by means of an area contraction near the downstream end of the driven section. Air is ionized by a unipolar corona discharge device comprising of a sharp-edged wedge as a high-field electrode inserted in a 41.25 mm (2") ID tube that forms a low-field electrode. The device requires less than 0.5 W. A ring probe, downstream of the corona discharge device, collects charges (ions and electrons) from the air; its output voltage is thus a measure of the degree of ionization. The degree of ionization is varied by varying the corona discharge voltage and the flow speed.

Corona generation was initially demonstrated with bench tests. These indicated an increased degree of ionization with an air flow created by a fan,

relative to that in static air. Tests in a shock tube, with subsonic and supersonic air flow, and with a negative corona, provided results with the same ionization behavior. The operating range of discharge voltages is relatively small for a positive corona; hence, shock tube tests were confined to a negative corona.

Shock tube test results indicate that, on a 10 millisecond time scale, corona generated ionization was convected downstream to the probe location in a supersonic flow. An anomalous shock tube result is a probe signal, without a corona discharge, that is similar, but weaker, to the signal with a discharge.

Although the tests were done with shock speeds up to about 1 km/s and with atmospheric air ahead of shock wave, the technique of ionization and plasma measurement can be extended to higher speeds and lower pressures. It is also suggested that a supersonic wind tunnel with a Langmuir probe be used for this type of work.

TABLE OF CONTENTS

LIST OF FIGURES

LIST OF TABLES

LIST OF ABBREVIATIONS

a	speed of sound, m/s
E	electric field, V/mm
M	Mach number
p	pressure, Pa
R	gas constant, J/kg-K
T	temperature, K
W	molecular weight of gas, kg/kg-mole
β	shock wave angle, degrees
γ	ratio of specific heats for a gas
θ	half wedge angle, degrees
μ	Mach angle, degrees
ρ	density, kg/m^3
τ	induced shear stress on the wedge due to pressure loading, Pa

Subscripts

0	stagnation property
1	gas upstream of the incident shock wave
2	gas traversed by an incident shock wave

3	gas region between a rarefaction wave and contact surface
4	driver gas
5	gas traversed by a reflected shock wave
6	sonic condition at the head of a rarefaction wave
7	gas downstream of the contact surface of the transmitted shock wave
8	gas downstream of the transmitted shock wave
9	gas downstream of an attached oblique shock wave
n	normal component
r	reflected shock wave
s	incident shock wave
t	transmitted shock wave

CHAPTER 1

INTRODUCTION

A proof-of-principle experiment is discussed for the generation of a steady corona discharge in a supersonic air flow. The experiment is performed in a shock tube where the strength of the incident shock wave is increased by its passage through a large area contraction located in the low pressure side of the tube. The increase in the shock Mach number is sufficient for the flow, downstream of the shock, to be supersonic. A corona discharge is generated in the low pressure side of the tube to ionize the supersonic air. The corona discharge ionization device (CDID) consists of a slender wedge with a sharp leading edge inserted into the tube forming high and low-field electrodes respectively [Figure 1 (a)]. The discharge between the leading edge of the wedge and the inner wall of the tube is generated by applying a high DC voltage between the electrodes. Typical discharge voltage and current values are 9.5 kV and 40 μA respectively. The discharge power is below 0.5 W. Thus, the corona is weak and the ionized gas is referred to as a cold plasma. The plasma is convected behind the incident shock. A ring probe, located in the downstream side of the wedge, measures the ionization level.

After the incident shock has passed the wedge, the supersonic flow passes through two weak, attached, oblique shock waves as shown in Figure 1(b). The Prandtl-Meyer expansion fans, generated at the base of the wedge, interact and weaken the oblique shock waves. Consequently, there is a minimal disturbance to the flow, although there is a wake flow downstream of the base of the wedge. The discharge is between the sharp leading edge of the strut (wedge) and the adjacent walls. Most of the ionization, however, occurs in the intense electric field that is local to the leading edge of the strut. The rate of generation of the ionization can be oscillatory with a high frequency, as will be shown later. For the purpose of this study, the average rate is equivalent to that of a steady corona discharge. The rate of ion-electron recombination is expected to be quite slow in a cold plasma. Ionized gas is thus convected downstream, primarily in the wake of the strut. This ionized wake constitutes a pre-ionizing "trigger" that sharply reduces the otherwise quite large breakdown voltage of the gas. Depending on the application, an array of struts would provide multiple layers of pre-ionized gas in the downstream flow.

A possible application of interest would be for a hypersonic air-breathing engine that utilizes an array of intense arcs between relatively widely separated walls. Each arc would initiate a detonation wave in a fuel/air mixture inside the supersonic, ionized wake flow. With a wall separation of perhaps 10 cm, a very large breakdown voltage is required for an arc. For sea-level air, the breakdown

voltage is about 11.5 kV/cm.[1] With pre-ionization, however, this value is expected to be sharply reduced; the resulting arc is now intense and reproducible. Despite the high speed of the flow, a system of detonation waves would rapidly merge and process a slug of combustible gas before the gas enters a thrust nozzle. Other possible applications for a steady, pre-ionized, supersonic flow would include electronically excited, supersonic lasers[2] and magneto-hydrodynamic (MHD) shock, or wind, tunnels.[3,4]

Alternative ionization methods, e.g., would include seeding the gas with sodium or cesium[5] or using an electron beam.[6,7] With the current approach, pre-ionization by a corona discharge has a number of advantages:

(i) steady operation at a high pressure,

(ii) small power requirement,

(iii) modest disturbance to the gas flow, and

(iv) simple to implement.

Still other features are discussed shortly.

A corona is a special type of glow discharge. It may be AC or DC; hereafter, only a DC discharge is of interest. The corona is referred to as unipolar when the field strength is large at only one electrode, as is the case shown in Figure 1. If the intense field is at the anode (cathode), the corona is a positive (negative) discharge. A weak corona is distinct from other types of glow discharges in having, at least, one electrode with a small wall curvature (sharp

point, sharp edge, or thin wire), and a large voltage difference between electrodes, but with a very small current. Hence, the electric power requirement is quite modest, and the ionized gas is considered to be a cold plasma. For instance, in the subsequent experiments, the maximum values for the voltage and current are 9.6 kV and 40 μA, respectively, with a maximum input power of only 0.4 W. While sufficient for ionization, it is insufficient for the direct initiation of combustion in an air/fuel mixture and for generating a discernible pressure disturbance.

A corona wind is used to enhance forced convection in an incompressible flow.[8] From Reference (8), it is known that a positive corona is stabilizing for the flow, whereas a negative corona is destabilizing. In other words, with a negative corona, the flow can become turbulent, if it is not already. In a unipolar positive corona, Reference (9) demonstrates that the electrons are concentrated inside the intense field about the anode, while the ions are distributed throughout the region containing the rest of the field. In a unipolar negative corona, the positive ions are concentrated inside the intense cathode field, while the electrons are distributed throughout the region containing the rest of the field.

Corona discharges are a relatively common phenomenon.[10,11] They can be detected by a faint glow (in a darkened room), a distinct buzzing sound, and by their ozone odor.[12] Quantitatively, a Langmuir probe can be used to measure the plasma.[9]

Depending on the application, a corona discharge may have several useful features, in addition to those previously mentioned. For instance, the stabilizing feature is useful with a supersonic laser. On the other hand, for the generation of a detonation wave (using pre-ionization) in a combustible mixture, both destabilization and ozone are advantageous. Ozone dissociates to O_2 and O, where the oxygen atom radical is effective in reducing any ignition delay time.[13] Autoignition at a hot spot is enhanced by turbulent mixing,[14] which can reduce the time from arc energy deposition to the formation of a detonation wave.

As indicated by several of the preceding references, there is a considerable body of literature dealing with corona discharges. The author, however, is unaware of existing publications in which a weak corona is generated inside a steady, supersonic gas flow. For instance, Yano, et al.,[15] discuss a subsonic glow discharge that becomes supersonic after passing through a nozzle throat. The discharge is not a corona, since neither electrode has a small curvature and the input power is 680 W. Similarly, the discharge is not a corona in Ershov, et al.[16] It occurs between electrodes located outside of a low pressure, supersonic plume and the current exceeds 1 A. In Leonov, et al.,[17] a high frequency discharge occurs in a supersonic flow by means of filaments in which the power into a single filament is at least 1 kW. A filament appears to originate at the sharp leading edge of a flat plate and then is convected downstream while it remains normal to the plate. The corona, however, is not weak, steady, or a cold plasma.

Although referred to as a corona, it is not, since the power level is too high and the electrode does not have a small curvature. Finally, in References 18 and 19, the discharge is generated in a subsonic flow.

The next chapter describes the technique used to ionize supersonic air by means of a corona discharge. Also described is an existing shock tube suitably modified to include the ionization device.

Bench tests were initially conducted to demonstrate the presence of a corona. The bench tests were also necessary to determine a suitable ionization voltage with the present configuration, to get as high an ionization intensity as possible. A plasma diagnostic, adaptable to the supersonic flow condition in the shock tube, is utilized during these experiments.

Chapter 3 discusses experimental results for bench and shock tube tests and analysis of the results is also provided. The results exhibit a sustained plasma in a supersonic flow. They also indicate the necessity for improving the instrumentation technique. An anomaly is discussed that should be deciphered.

Finally, in Chapter 4, a number of recommendations are made to improve the instrumentation and operation of a corona ionization device.

CHAPTER 2

EXPERIMENTAL FACILITY AND PROCEDURES

2.1 Generation of supersonic air flow

2.1.1 Concept

A shock tube is used to generate a high-speed flow downstream of a normal shock wave. A desired shock speed is obtained by charging the driver section with dry air at a suitable high pressure, while the initial pressure of the driven section is atmospheric air. The driver and driven tubes are separated by an intermediate double-diaphragm section, which initially is charged with air at about half the driver pressure. Both diaphragms rupture upon venting the intermediate section. A shock wave is generated with supersonic air flow behind it that propagates downstream through a test section containing a corona discharge. It can be shown[20] that the incident shock Mach number needs to be greater than 2.07 to generate a downstream supersonic flow. There is a sudden contraction inside the driven tube, which results in an increase of the shock speed[21] of about 15 - 18%. The smaller cross-sectional area tube downstream of the contraction contains an ionization device for generating a corona discharge.

Figure 2 shows a shock tube with an area contraction and a corresponding wave diagram. Regions 1 and 4 contain the initial low and high pressure gases in the driven and driver sections, respectively. The low pressure side of the tube is open to the atmosphere for all tests; hence, its initial pressure is taken as 10^2 kPa. The cross-sectional area to the left of state 6 is A_L, while to the right it is A_R; the area contraction ratio is $\alpha = A_L / A_R$. (See the List of Abbreviations for the definition of symbols.) The incident shock wave partly reflects from the contraction thereby giving rise to region 5. Part of the incident shock propagates into the small diameter tube with a Mach number M_t, which is larger than the incident Mach number M_s.[21] Region 8 is a uniform flow region between the transmitted shock and the contact surface, labeled *CST*. Pressure and velocity tangency conditions apply across *CST*. Region 7 is also a uniform flow region. A rarefaction wave is required between states 6 and 7 in order for the relatively high pressure flow at 6 to adjust to the state 7 pressure. The leading edge of the wave is fixed at state 6 and is sonic.[22] It is analytically established[21] and experimentally verified that the transmitted shock Mach number M_t is larger than the incident shock Mach number M_s by about 15 - 18%.

2.1.2 **Technique to get a desired shock Mach number M_s**

The basic parameter that governs shock tube operation is the diaphragm pressure ratio p_4 / p_1 given by

$$\frac{p_4}{p_1} = \frac{p_2/p_1}{\left[1 - \frac{(\gamma_4 - 1)\frac{a_1}{a_4}\left(p_2/p_1 - 1\right)}{\left(4\gamma_1^2 + 2\gamma_1(\gamma_1 + 1)\left(p_2/p_1 - 1\right)\right)^{1/2}}\right]^{2\gamma_4/(\gamma_4 - 1)}} \quad (1)$$

where

$$\frac{p_2}{p_1} = 1 + \frac{2\gamma_1}{\gamma_1 + 1}\left(M_s^2 - 1\right) \quad (2)$$

For air on both sides of the diaphragm section, the specific heat ratios, γ_1 and γ_4, equal 1.4. The pressure ratio p_4/p_1 is a function of M_s as well as a_1/a_4. Since the driven gas is air at room temperature, a_1 is fixed; M_s is then dependent on p_4/p_1 and a_4. Hence, there are two ways by which a value for the pressure p_4 can be computed:

(1) For a given driver gas, a_4 is fixed and p_4 can then be obtained for a desired M_s value by choosing p_1. Table 1 provides theoretical values for p_4 for M_s = 2.5, 3, 3.5 and 4 when p_1 is specified. To operate the tube at a high Mach number value, it is necessary for p_1 to be sub-atmospheric.

(2) The pressure ratio p_4/p_1 can be reduced appreciably for a given M_s value by employing a driver gas with a large acoustic speed a_4 as compared to

a_1. Table 2 provides theoretical data for M_s ranging from 2 to 4 with driver/driven gases of air/air and helium/air. It is evident that when helium is used as the driver gas, p_4 is appreciably reduced.

Table 3 provides theoretical values of the parameters on both sides of the area contraction, with air as the driver and driven gases (see the Code in Appendix A). For instance, with p_4 equal to 145 bar and p_1 at one atmosphere, M_s equals 2.5. With an area contraction of 13.65, it is possible to have a transmitted shock Mach number M_t of about 2.96 and a Mach number of 1.35 in region 8.

2.1.3 **Shock tube facility**

Figure 3 shows the layout of the shock tube facility. The high performance shock tube consists of a high-pressure driver tube, a double-diaphragm intermediate section, and a driven tube with an area contraction ratio of 13.65. Dry air from a 6.9 MPa (1000 psi) compressor is further pressurized up to 31 MPa (4500 psi) using a Haskel pump. This high pressure air is stored in a spherical receiver for charging the driver tube (152.4 mm ID, 3.05 m long) and the diaphragm section. The intermediate section (152.4 mm ID, 0.114 m long) is charged with air at about half the driver pressure. This section is vented at the start of a run; the double diaphragms eventually burst and a shock wave is generated in the driven tube. The driven tube consists of two sections in which the first has an ID of 152.4 mm and a length of 8.344 m. The second section is a

2.188 m long 304-stainless steel tube with an ID of 41.25 mm and is open to the atmosphere at its end. This length includes the test section, which is the corona discharge device (Figure 4). The pressure rating of the 152.4 mm ID tube is 408 atm (6000 psi) and that of the 41.25 mm ID tube is 188 atm (2800 psi).[23] The area contraction α equals 13.65.

The 254 mm x 254 mm square diaphragms are constructed from 10 gauge hot-rolled 1008 steel plates, scored to various depths. Figure 5 illustrates the scoring pattern.

2.2 Generation of a corona discharge

2.2.1 Principle

A low temperature plasma is produced by means of a corona discharge, which is initiated by creating a field strength high enough to exceed the corona breakdown field strength for air. A high field strength is produced near a sharp point or edge of a conductor by charging the conductor to the required voltage, which then becomes a high-field or active electrode. The other electrode called the low-field or passive electrode can be a plate, rod, or a tube. Intense ionization is limited to a small region near the active electrode.

2.2.2 Facility

A unipolar type of DC corona discharge ionization device (CDID) was built to investigate the presence of charged particles in a supersonic air flow. Figure 6 illustrates the CDID, which consists of a stainless steel wedge whose

sharp leading edge is the high-field electrode (Figure 7). The wedge is inserted transversely into a stainless steel tube that is the low-field electrode. This tube has an ID of 41.25 mm, OD of 50.8 mm and a length of 362 mm. Insulation between the two electrodes is cast from a pourable, two-part urethane rubber, liquid Flexane 94, that has a high dielectric strength and a high temperature capability.

The assembly is connected to the stainless steel section with the leading edge of the wedge facing the incoming flow. Lexan tubes (127 mm long, ID 41.25 mm) are mounted at both ends of the CDID to electrically isolate the CDID assembly from the rest of the shock tube. A 12 kV D.C. supply is used to charge the electrodes that generate a corona discharge at the sharp leading edge.

2.3 **High-field electrode**

2.3.1 **Discussion**

A wedge-shaped electrode for corona discharge generation, in contrast to a traditional wire or rod-type electrode, is favored for the following reasons:

(a) The wedge is inserted with the sharp leading edge facing the incoming flow, transversely inside a steel tube that forms the low-field electrode. This configuration easily withstands supersonic aerodynamic loading. It also causes a minimum perturbation of the high-speed flow. The wedge is secured, along with insulation, to the tube by means of clamps.

(b) The sharp leading edge of the wedge results in a high field intensity at the edge.

(c) Attached oblique shock waves at the leading edge of the wedge are weaker than a detached bow shock.

(d) The cross-sectional area is designed to resist transverse shear at the fixed ends, caused by the aerodynamic loading of the supersonic flow.

2.3.2 **Geometry**

Based on the above considerations, the following wedge design was selected [Figure 6(a)]:

wedge angle = 2 θ =14.25^{o}

wedge base width = b = 4.76 mm

median of the triangular section = a = b / (2 tan θ) = 19 mm

length of the wedge along the sharp edge = 191 mm

For a deflection angle θ = 7.125^{o}, an attached oblique shock is possible for upstream Mach numbers above 1.32.[24] Table 3 provides values for the following parameters for an incident shock Mach number M_s of 2.5:

M_t = 2.96

M_8 = 1.35

p_8 = 1007 kPa corresponding to p_1 = 100 kPa

From oblique shock theory, the pressure behind the oblique shock at the wedge is p_9 = 1.45 p_8 = 1460 kPa. Figure 8 shows the aerodynamic pressure loading on the wedge. The unknown base pressure is conservatively assumed to be zero. The fluid force F on the wedge in the flow direction is given by

$$F = 2\ p_9 \frac{a}{\cos\theta}(ID\ \ of\ the\ \ tube)\sin\theta$$

where

$\theta = 7.125^{o}$,

$ID\ \ of\ the\ \ tube = 0.04125$ m,

$F = 1.958 \times 10^{-4}\ \ p_9 = 0.286$ kN

The induced shear stress on the cross section is

$$\tau = \frac{F}{2(cross-sectional\ \ area\ \ of\ the\ wedge)}$$

where

$$cross-sectional\ \ area = \frac{ab}{2} = 4.5 \times 10^{-5}\ \ \text{m}^2$$

This results in τ = 3.18 MPa, which is much less than the yield strength, 276 MPa, of the AISI annealed stainless steel.

2.4 **High-voltage DC power supply system**

2.4.1 **Transformer-capacitor circuit**

Figure 9 is a schematic of the small diameter tube including the test section. A power supply unit, capable of up to 12 kV DC, is shown in Figures 10 and 11. A variable autotransformer, connected through an isolation transformer to the 120 V, 60 Hz main supply, is used to vary the AC output of the 12 kV (rms), 60 mA neon-sign transformer from 0 to 100 %. The output of the neon transformer is rectified by means of a full-wave bridge rectifier that consists of 4

diodes with a peak inverse voltage rating of 125 kV each. The AC ripples in the output of the bridge rectifier are filtered and charge stored in a 1 μF, 50 kV capacitor. Since the corona discharge current is of the order of 40 μA, the capacitor is capable of a slow discharge, thereby providing a near steady DC voltage for the CDID.

Four resistors, in series, with a total value of 500 MΩ are connected across the capacitor to prevent the capacitor from discharging too quickly when the neon transformer is isolated. The time constant for the RC network is RC = 500 MΩ x 1μF = 500 seconds. Thus, the capacitor took 500 seconds to lose 63 % of its original value. As the run time is several tens of milliseconds, the steady power supply duration is satisfactory.

A maximum voltage of 14 kV DC is obtained with the neon transformer of 12 kV AC. The peak voltage level of the transformer is

$$V_p = \sqrt{2}\,V_{rms} = \sqrt{2} \times 12 = 16.97 \;\; kV$$

A voltage drop of about 4 kV is observed across the diodes making available a net DC voltage of about 13 kV. However, the maximum voltage required for the experimental study is about 11 kV and this voltage drop is acceptable.

2.4.2 **H.V. relays for charging and discharging**

The power to the wedge-tube electrode configuration is applied through a pair of high-voltage fast-acting relays with 15 ms response time (Figure 11).

These relays can be triggered simultaneously and they operate on 12 V DC. The current limiting resistor (1.1 MΩ) on the output side of the capacitor prevents arcing. As noted, the discharge current is of the order of 40 μA. The voltage drop across this resistor is negligible (about 0.5%). Another pair of relays in series with a resistor of 200 kΩ is provided to discharge the capacitor. The total resistance in this RC circuit during discharge amounted to 1.3 MΩ giving a time constant of 1.3 s. Thus, the capacitor can be discharged quickly at the end of a test.

2.5 **Instrumentation**

The large diameter driven tube is instrumented with two flush-mounted pressure transducers PT2 and PT3 as shown in Figure 4. These dynamic PCB model 111A24 transducers have a full-scale pressure range of 68.9 atm. They have a voltage sensitivity of 5 mV/psi with a 400 kHz resonant frequency, a time constant of 100 s, and a rise time of 2 μs. The transducers are mounted at distances of 6.185 m and 7.531 m from the diaphragm section. The transducers are used to obtain the pressure of the air behind the incident shock wave at two axial locations along the shock tube. The incident shock speed is calculated using time-of-flight data between these two locations. The incident Mach number M_s is calculated from the known ambient conditions present in the driven tube. The pressure p_8 behind the transmitted shock wave and the transmitted shock Mach number M_t are then obtained using the annotated code (Appendix A) that also produced the data in Table 3.

Transducers monitored the transient conditions in the driven section during a run. Data sampled by the transducers are recorded with a 48-channel data acquisition system (DSP Technology) interfaced with a personal computer at a sampling rate of 100 kHz/channel with 12-bit resolution.

The data acquisition system is triggered externally to record data during the air flow. A pressure transducer PT1, mounted on the driven tube at a distance of 2.22 m from the diaphragm section (Figure 4), is used to trigger the data acquisition system. This pressure transducer is connected to the triggering circuit of the data acquisition system through a signal conditioner. An amplifier is used in the triggering circuit to suitably amplify the output of the pressure transducer.

The voltage across the capacitor, which is also the corona discharge voltage, is measured by means of a high impedance, digital DC voltmeter connected across a voltage divider as shown in Figure 11. The total resistance is 500 MΩ. A voltmeter, connected across a 5 MΩ resistor, thus has a multiplying constant of 100. A bi-directional 50 μA (and a 100 μA/200 μA not shown) DC analog ammeter, in series with the test section, measures the discharge current.

Charged particles in the supersonic air plasma cause an electric current to flow through a ring probe attached to the test section as shown in Figure 9. The ring probe is located 368 mm from the leading edge of the wedge in the test section. It is made of oxygen-free copper having a width of 9.53 mm. Its ID and OD are the same as the Lexan insulator. It is isolated electrically on both sides by

1.59 mm thick Teflon rings. Voltage output from the ring probe is measured across a 100/333 kΩ resistor. Output from this resistor is captured after amplification as pulsed signals using a HP 54542A digital storage oscilloscope that has a maximum sampling rate of 2 GHz. The sampling rate used for the study is 25-100 kHz, with a record length of 2048 - 8192 samples. The low-frequency noise rejection feature of the oscilloscope is used to minimize the influence of the AC noise signal received by the ring probe. The oscilloscope is triggered by the output of the triggering pressure transducer PT1 simultaneously with the triggering of the data acquisition system.

2.6 **Experimental procedure**

2.6.1 **Bench tests**

Bench tests of the ionization device at atmospheric pressure were conducted prior to shock tube tests to obtain discharge voltage versus discharge current characteristics and the discharge voltage versus ring probe output characteristics. Figure 12 is a photograph of the apparatus. Charged particles attracted to the ring probe (referenced to the ground) cause a current to flow through the probe circuit. Current is obtained by measuring the voltage across a precision resistor in the probe circuit. Tests were performed to ascertain the maximum discharge voltage that could be applied to the CDID without arcing. These were conducted over a 0-10 kV voltage range across the electrodes both in static air and with air blown through the device by a small fan set at its maximum

speed (Figure 12). Tests with air blown by the fan ascertained the effect on the probe output of air flow past the ionization section.

Ionization at the leading edge of the wedge is demonstrated by visible tiny corona glow points along the leading edge (Figure 13), by feeling the ionic wind convected along the tube, and by a buzzing sound. Ozone odor, produced during ionization, is also sensed. A high voltage, low current discharge, confirms the ionization. The pulsed nature of the probe output also demonstrates the unsteadiness of the ionization process.

Output of a single ring probe is captured by an oscilloscope for each discharge voltage. Corona discharge voltage and corresponding current are also measured. The RMS value of the probe output voltage is calculated. Tables 4 and 5 show bench test data for both negative and positive coronas. Figures 14 and 15 show the corona discharge characteristics and the ring probe characteristics obtained from this data. The probe output of a positive corona is large enough to be measured without an amplifier unlike that of a negative corona, which requires an amplifier with a gain of 100. The probe output of a positive corona is also obtained with the same amplifier used for the negative corona in order to compare the two. Figures 16(a) and (b) show the relative characteristics of negative and positive coronas. Figure 17(a) and (b) show the ring probe signal with and without air flow from the fan for a negative corona.

2.6.2 **Shock tube tests**

Tests were conducted with the CDID installed in the shock tube. A catalogue of tests is provided in Table 6. Only test runs with proper triggering and diaphragm ruptures are listed. Figure 18 is a photograph showing part of the shock tube and instrumentation. Discharge and probe characteristics are necessary with the new setup. These characteristics differ from those for the bench tests. A comparison can be made between the ionization intensity in static air and that for a region 8 (Figure 2) with subsonic or supersonic air flow.

Static tests with a corona discharge were conducted for discharge voltages varying from zero to 9.6 kV (Run 1 in Table 6). Figure 19(a) shows the corona discharge characteristic. The configuration of the CDID is a little different from the one in the bench test, due to its extended length in the shock tube; hence, there is a small difference between the two results. Figure 19(b) (Run 1) shows V_{rms} from ring probe data (from the oscilloscope) versus the discharge voltage. Figures 20(a) and (b) show, for this run, oscilloscope traces of signals of static air ionization. Static tests were conducted for both negative and positive coronas. It is observed that for a positive corona, a measurable ionization intensity occurs only for voltages above 9 kV, and arcing would take place if the voltage exceeds 9.5 kV. Arcing is accompanied by a cracking sound inside the CDID and by the micro-ammeter needle deflecting beyond the meter's range. Hence, it was decided to conduct shock tube runs only with a negative corona.

Tests were conducted with a subsonic flow downstream of the incident shock, and with corona discharges at about 9 kV. From previous negative corona static tests, it was known that a high intensity of ionization occurs at about 9 kV without arcing. Unscored aluminum diaphragms of thickness 0.4 mm were used to generate a subsonic flow. Driver and driven pressures were 1.28 MPa (185 psi) and 100 kPa (14.5 psi), respectively, before venting the intermediate section of the tube. The PT2 and PT3 data are used to evaluate the shock Mach number M_s with the time-of-flight method. The transmitted shock Mach number M_t and the flow Mach number M_8 following it are obtained according to Reference (21). Figure 21(a) shows data (Run 6), from the PT2 and PT3 transducers, where pressure jumps due to the incident and reflected shocks are evident. Ring probe output is amplified with a gain set at 10. Figure 21(b) shows the output for a negative corona at 9 kV (Run 6). Figure 21(c) is an expanded diagram of the ring probe output for the indicated duration. Video pictures were taken using a surveillance camera during a run to observe the changes in the discharge voltage and current and the oscilloscope wave-form image.

Tests (Runs 7-9) were conducted with supersonic flow, initially with a negative corona discharge in the voltage range of 8 to 9 kV, and with scored steel diaphragms. The driver pressure was in the range of 13.1-15.1 MPa with atmospheric air on the driven side of the tube. Figure 22(a) shows pressure transducer data for Run 9. The corona discharge, for this run, is 8.55 kV at the

time of diaphragm rupture. Shock Mach numbers M_s and M_t, and the flow Mach number M_8 are then obtained as described previously. As can be seen from Figures 22(b) and (c), the ring probe output (Run 9) saturates. This is because the signal is amplified (with a gain of 10 set in the amplifier) beyond the limits set in the oscilloscope.

A probe signal duration of about 60 ms may seem excessive, e.g., see Figure 22(b). This is a consequence of a relatively long tube length (13.58 m), moderate M_s and M_t Mach numbers, and a large area contraction. The contraction generates, for instance, a significant reflected shock wave with its downstream flow moving toward the high-pressure end wall.

To ascertain if there is a probe signal for a supersonic flow without a corona discharge, the tube was run without applying any excitation to the CDID (Run 10). The driver pressure was set at 14.48 MPa with atmospheric air on the driven tube side. The unexpected result (Figure 23) shows an output that appears to be almost the same as the one with a corona (Run 9), with other conditions the same. In both cases, the signal does not require amplification beyond that provided by the oscilloscope. It was then decided to do away with the amplifier in the ring probe circuit and to capture the output within the limits of the oscilloscope. Tests (Runs 11 and 12) were carried out with supersonic flows with the same driver pressure and with and without a negative corona initially at 9.55 kV. Figures 24 and 25 show results with and without a corona, respectively. RMS

values of the output for the duration of 12 to 50 ms are indicated for these runs on the plots. A test (Run 14) was also conducted for a subsonic flow without a corona with the driver pressure equal to 128 kPa (185 psi). Figure 26 shows the corresponding data with V_{rms} (un-amplified) for the duration of 17 to 47 ms.

To establish if a flow contains a greater intensity of charges compared to that in static air with a corona, it was necessary to investigate, in the shock tube, the V_{rms} of the output for a corona at the same initial discharge voltage of 9.55 kV used in static air. Figure 27 gives the result from a static test (Run 13).

A detailed analysis of the results from various tests is given in the next chapter.

CHAPTER 3

EXPERIMENTAL RESULTS AND DISCUSSION

3.1 Bench tests

The following observations are based on bench test results.

1. Tables 4 and 5, as well as Figures 14 and 15, show that the starting voltage for a negative corona is nearly 8 kV whereas that for a positive corona it is about 9 kV. Arcing occurs between the electrodes at 10 kV for both coronas; hence, subsequent testing did not go beyond 9.55 kV.

2. It is observed from Figures 14(a) that airflow with a negative corona discharge at 9.5 kV reduces the discharge current from 24 μA to 15 μA. This conductivity decrease stems from the stretching of field lines by the airflow. This is confirmed by the increased probe output [Figure 14(b)] during flow compared to a static air output for all voltages up to 9 kV. Figures 15(a) and (b) show a similar trend in the case of a positive corona. The output slightly decreases for voltages above 9 kV for a negative corona, possibly due to a higher rate of recombination. Figures 17(a) and (b) show a pulsed output for a 20 ms period in the case of a negative corona at 9 kV, without and with airflow, respectively. The respective V_{rms} outputs are 0.51 V and 0.76 V. This indicates that the plasma contains more charges with a flow.[25]

3. The probe output is significantly larger for a positive corona than it is for a negative one, at a large discharge voltage, as seen in Figure 16(b). This indicates a greater ionization intensity with a positive corona. Since the operating range for a positive corona with the present electrode configuration is small (9.25 to 9.5 kV) compared to a negative corona, the subsequent shock tube investigation was carried out only for a negative corona.

The negative corona decision has two consequences. First, the discharge is appreciably weaker. Second, as noted in the Introduction, positive ions, rather than electrons, are concentrated around the wedge's sharp edge in a negative corona.

3.2 **Shock tube tests**

A primary objective of this study is the detection of a plasma in supersonic flow. The data obtained from several runs are compared and discussed as outlined below.

Figures 19(a) and (b) show the corona discharge and the ring probe output characteristics from a static test (Run 1) on the CDID in the shock tube with a negative corona. These are a little different from Figures 14(a) and (b) due to the changed configuration for the CDID in a shock tube. The configuration change arises from the extended length of the CDID, on both sides, on mounting it on the shock tube. Figures 20(a) and (b) show a pulsed output for each corona at discharge voltages of 6 and 8 kV.

In the case of subsonic flow (Figure 21, Run 6), with a negative corona at 9 kV, M_s is found to be 1.66 (time-of-flight). The transmitted shock Mach number in the small diameter tube is evaluated[21] at 1.95, which results in $M_8 =$ 0.931. The pressure and temperature downstream of the transmitted shock are 426 kPa and 482 K, respectively. Figure 21(b) (Run 6) shows that the RMS value of the probe output, V_{rms}, amplified with a gain of 10, equals 156 mV. The unamplified V_{rms} output is thus 15.6 mV. Figure 26 (Run 14) shows the unamplified V_{rms} output, for an equivalent run without a corona, equals 12 mV, for the same interval of run time of 17 to 47 ms as that chosen for Run 6. This interval excludes the effect of the shock wave and is sufficient to provide a meaningful result. A difference of 3.6 mV between these runs suggests the possibility of the flow sweeping downstream charges from the CDID ionization region.

For the case of supersonic flow (Run 9), with the driver and driven tube pressures at 14.5 MPa (2100 psi) and 100 kPa (14.5 psi), the incident shock Mach number in the large diameter tube is found to be 2.5. The transmitted shock Mach number in the small diameter tube is evaluated[21] at 2.96, which results in $M_8 =$ 1.35. The pressure and temperature downstream of the transmitted shock are 1 MPa and 790 K, respectively.

For a supersonic flow with and without a corona, the V_{rms} probe output, is considered for the time interval of 12 to 50 ms. This interval excludes the effect of

the shock wave and is sufficient to provide a meaningful result. Figures 24 and 25 (Runs 11 and 12) show V_{rms} values, with and without a corona at 9.55 kV, as 326 mV and 310 mV, respectively.

The high intensity of the output, for a subsonic or a supersonic flow without a corona from the CDID, suggests the existence of some other source for the generation of electrical charges picked up by the probe. Note that the supersonic flow with a corona contains a 16 mV (between Runs 11 and 12) larger charge than one without corona; the same trend occurs in the case of a subsonic flow. This difference in output is not due to any source other than the corona from the CDID.

The V_{rms} probe output from a static test (Run 13) with a corona at 9.55 kV, for a run time interval of 12 to 50 ms, is 9 mV (Figure 27). By comparing this value with the 16 mV mentioned above suggests that supersonic flow contains a greater number of charges than static air.

Figures 14(b), 15(b), and 17(a) and (b) show a similar behavior, in the case of bench tests; an increased intensity in the output signal because of flow.

It is also observed that the current goes to zero momentarily after the shock wave passage. Since the discharge voltage between the electrodes is still in the vicinity of 9-9.5 kV, a condition of zero discharge current indicates that there is an insufficient charge-intensity between the electrodes to maintain conductivity.

This leads to the same conclusion as mentioned in the case of subsonic flow; the flow sweeps ionized gas downstream[6].

During a test (quiescent, subsonic, or supersonic) the corona discharge voltage and current are visually monitored by a surveillance camera. As noted, the voltage slowly and smoothly decreases from its pre-test charged value. A gradual change is not the case for the discharge current for either a subsonic or a supersonic test. As soon as the crack associated with diaphragm rupture is heard, the microammeter current is observed to sharply drop from its pre-rupture value of about 40 μA to a zero, or near zero, value. After the minimum value occurs, the ammeter reading rapidly increases to a value below its initial value, in accordance with the steady decrease in the discharge voltage. The response time of the ammeter and its circuit is unknown. Hence, the actual time interval, between when the current reading starts to decrease until it recovers, is unknown. This time interval would be meaningful if the recorded response time of the meter and its circuit is no more than 0.1 ms. The initial current decrease is interpreted as indicating the time when the transmitted incident shock passes over the wedge. The shock and its immediate downstream flow proceed to sweep the ionized gas with it, thus extinguishing, or nearly extinguishing, the corona. The subsequent increasing current indicates, however, re-establishment of the corona, but now in a high-speed flow.

Figures 28(a)-(c) (Run 12) demonstrate this behavior. Figure 28(a) shows the microammeter with a value of about 35 μA, while the discharge voltmeter has a 9.67 kV value. Right after the shock passes by the wedge, [Figure 28(b)], the meter has a near zero value when the discharge voltage is 9.55 kV. Figure 28(c) shows that the meter has a slightly larger value at a later time.

A sudden increase in the ring probe output [Figures 21(b), 21(c), 24 and 25], at the instant of shock passage through the CDID, is significant for subsonic and supersonic flows. A similar observation was also recorded in previous research[5] but no definite reason was attributed to this.

A number of possible reasons are discussed for the observed probe signal during a flow without a corona and for the signal spikes at the time of the shock passage. Hard tapping on the CDID tube with a hammer was done without flow and without a corona. An amplifier, with a gain set at 100, was connected in the ring probe circuit. A delayed spike in the output signal, a little time after continuous 5/6 blows at the probe end of the CDID, is observed. This delay is due to the slow response of the amplifier, and suggests generation of charges from an electromechanical source, such as the piezoelectric property of a material. From several sources of information,[26] it is found that Teflon, used to insulate the ring probe on both sides, is a piezoelectric material. Other possible reasons for the probe signal, such as the influence of Lexan insulation material, were considered.

The mechanism of ionization behind a shock wave was also studied to explore its possible contribution to the ring probe output.

3.3 **Uncertainty analysis**

Data uncertainty arises from measurement errors. Limitations of the data acquisition equipment, sensors, and instruments contribute to the data acquisition errors. The uncertainty analysis employed here is based on the method given in the Reference (27). Let R be the desired result of an experiment; it is given as a function of a set of measured variables x_1, x_2, x_3,…. Let w_R be the uncertainty in the result and w_1, w_2, w_3,… be the uncertainties (known) in the variables. Then the uncertainty in the result is given by

$$w_R = \left[\left(\frac{\partial R}{\partial x_1} w_1 \right)^2 + \left(\frac{\partial R}{\partial x_2} w_2 \right)^2 + \left(\frac{\partial R}{\partial x_3} w_3 \right)^2 + \ldots \right]^{1/2}$$

The manufacturers' specifications of transducers and sensors are used for the uncertainties of the variables.

Table 7 lists the experimental parameters measured and acquired along with their uncertainties. The only result that is evaluated is the shock Mach number given by

$$M_s = \frac{w_s}{a_1}$$

The shock speed is determined by the time-of-fight (TOF) method and is given by

$$w_s = \frac{\Delta L}{\Delta t}$$

where ΔL is the distance between two transducers, PT2 and PT3, and Δt is the time for the shock wave to propagate past the two transducers. The sonic velocity corresponding to the ambient conditions is given by

$$a_1 = (\gamma R T_1)^{1/2}$$

The variables involved in the above relation for the shock Mach number are thus ΔL, Δt, and T_1.

The uncertainty in the measurement of ΔL is $\pm$ 0.001 m. The uncertainty in the measurement of time Δt, referred to the peaks of the pressures obtained from the data acquisition system, is taken as $\pm$ 0.013 ms. The uncertainty in the measurement of the temperature T_1 is $\pm$ 1 K. The maximum uncertainty in the evaluated shock Mach number M_s, from the equation for uncertainty given above, is found to be $\pm$ 0.7 %. This shows the TOF method used is precise enough to obtain the incident shock Mach number.

The uncertainty in the measurement of the voltage, V_{rms} in the oscilloscope, from the manufacturer's specification, is $\pm$ 1.3 %. Other parameters measured are the discharge voltage, V and current, I. The voltmeter is a digital-type meter and the ammeter is analog-type one. The uncertainties of these were found to be $\pm$ 1 % and $\pm$ 2 % respectively.

CHAPTER 4

CONCLUSION AND RECOMMENDATIONS

Based on the previous discussion, the following conclusions are made.

1. Results from the shock tube tests confirm that a plasma generated by a corona discharge sustains itself in a subsonic or supersonic flow.

2. The rate of ionization is greater for a positive corona compared to a negative corona. With a modified configuration, such as increasing the smallest distance between the electrodes, it is possible to have a wider operating range of discharge voltages for a positive corona without arcing.

3. Supersonic air at the downstream end of the CDID contains a greater charge density than when subsonic.

4. An investigation should be considered into the reasons behind the generation of a probe signal with high speed air flow in the absence of ionization due to a corona. A series of ring probes, Teflon insulated, were used in the shock tube ionization (by seeding) studies of Reference (5). They did not check, however, on the probe signal when ionization was not present.

The possibility of ionization behind a shock wave is first considered. Extensive investigations[28-30] were carried out on ionization behind shock waves in

air and other gases like argon. Details of the mechanisms that produce the ionization behind a shock wave are available.[28] Experiments carried out were at shock speeds above 5 km/s and at low pressures on the order of 1 mm of mercury or even less.

In contrast, the experiments carried out here had a maximum shock speed of about 1 km/s into atmospheric air. Literature for these conditions, which would indicate that dissociation occurs, no less ionization, could not be found. The reason, of course, is that the maximum post-shock temperature is only about 800 K. At this temperature, only a modest fraction of the oxygen molecules are vibrationally excited. Post-shock dissociation, and certainly ionization, cannot occur.

Teflon, being a piezoelectric material,[26] could be a source of the non-corona signal generated during propagation of a shock wave and high speed air flow. Since the ring probe is in direct contact with the Teflon rings on its sides, it is more likely the source than Lexan insulation or charged particles on the inner surface of the tube wall.

Based on the experimental work undertaken and the results obtained from it, the following suggestions are put forth.

1. It would be useful to investigate the signal generated due to a high speed flow in the shock tube. The signal due to ionization by a corona is almost obscured by this non-corona signal; it is therefore difficult to convincingly prove

the success of this experimental work. One way of eliminating the non-corona signal, if due to the piezoelectric effect, is to replace the ring probe and its Teflon insulation with a Langmuir probe. A suitable sting is required to secure the probe. One of the reasons, for the selection of a ring probe in this work, is the ease with which it could be secured to the CDID. The other reason is to provide a greater area for collection of charges from ionization. It is now realized that a different kind of probe that does not give rise to a non-corona signal is vital, since the ionization signal due to a negative corona is small.

2. It would be useful to have a steady supersonic flow to conduct this experiment. A steady flow would establish if ionization is sustained downstream. Hence, a supersonic wind tunnel, with its plenum chamber raised to the necessary pressure and temperature, would be useful for this work.

3. A test for supersonic flow without a corona may be run by switching the positions of the ends of the CDID. This places both the Lexan insulators on the downstream side of the ring probe. The data from this would explain whether or not Lexan could be a possible contributor to the non-corona signal obtained before switching.

4. It is recommended that shock tube tests be conducted with the downstream section evacuated to a low pressure and with and without a corona. The results from these tests might shed light on possible explanations for the non-corona signal.

5. It would be useful to have the output of the microammeter recorded continuously during a shock tube run. The timing of the sudden variation in the discharge current would then provide information about its nature of association with the shock wave or supersonic flow.

APPENDIX A

CODE

Input to the code consists of M_s, γ, R, T_1, p_1, and α. Further details may be found in Reference 21. Several common Mach number functions are defined as

$$X = 1 + \frac{\gamma - 1}{2} M^2 \tag{1}$$

$$Y = \gamma M^2 - \frac{\gamma - 1}{2} \tag{2}$$

$$Z = M^2 - 1 \tag{3}$$

A number of preliminary calculations are as follows:

$$\frac{p_2}{p_1} = \frac{2}{\gamma + 1} Y_s \tag{4}$$

$$\frac{p_4}{p_1} = \frac{p_2 / p_1}{\left[1 - \dfrac{(\gamma_4 - 1)\dfrac{a_1}{a_4}\left(p_2 / p_1 - 1 \right)}{\left\{ 4\gamma_1^2 + 2\gamma_1(\gamma_1 + 1)\left(p_2 / p_1 - 1 \right) \right\}^{1/2}} \right]^{2\gamma_4 / (\gamma_4 - 1)}} \tag{5}$$

$$\frac{T_2}{T_1} = \left(\frac{2}{\gamma + 1} \right)^2 \frac{X_s Y_s}{M_s^2} \tag{6}$$

$$M_2 = \frac{Z_s}{(X_s Y_s)^{1/2}} \tag{7}$$

$$a_1 = (\gamma R T_1)^{1/2} \tag{8}$$

State 5 utilizes the following equations where M_5 and $\tilde{M}_r$ are iteratively found. A superscript (1) denotes a first estimate.

$$M_5^{(1)} = \left(\frac{2}{\gamma+1}\right)^{(\gamma+1)/[2(\gamma-1)]} \frac{1}{\alpha} \tag{9}$$

$$F_1(M_5) = \frac{\gamma+1}{2}(\alpha M_5)^{2(\gamma-1)/(\gamma+1)} - \frac{\gamma-1}{2}M_5^2 - 1 = 0 \tag{10}$$

$$\tilde{M}_r^{(1)} = \left[1 + \left(\frac{\gamma+1}{4}\right)^2 M_2^2\right]^{1/2} - \frac{3-\gamma}{4}M_2 \tag{11}$$

$$F_2(\tilde{M}_r) = M_5 - \frac{1 - \frac{\gamma+1}{2}\tilde{M}_r\left(M_2+\tilde{M}_r\right) + \frac{\gamma-1}{2}\left(M_2+\tilde{M}_r\right)^2}{\left\{\left[1+\frac{\gamma-1}{2}\left(M_2+\tilde{M}_r\right)^2\right]\left[\gamma\left(M_2+\tilde{M}_r\right)^2 - \frac{\gamma+1}{2}\right]\right\}^{1/2}}$$

$$= 0 \tag{12}$$

$$M_r = M_2 + \tilde{M}_r \tag{13}$$

$$\frac{p_5}{p_1} = \frac{2}{\gamma+1}Y(M_r)\frac{p_2}{p_1} \tag{14}$$

$$\frac{T_5}{T_1} = \left(\frac{2}{\gamma+1}\right)^2 \frac{X(M_r)\,Y(M_r)}{M_r^2}\frac{T_2}{T_1} \tag{15}$$

$$\frac{a_5}{a_1} = \left(\frac{T_5}{T_1}\right)^{1/2} \tag{16}$$

State 6 is given by:

$$\frac{a_6}{a_1} = \left(\frac{2}{\gamma + 1} X_5 \right)^{1/2} \frac{a_5}{a_1} \tag{17}$$

M_t and a_7 / a_1 are iteratively given by two coupled equations

$$M_t^{(1)} = 1.15 M_s \tag{18}$$

$$\left(\frac{a_7}{a_1} \right)^{(1)} = 1 + \frac{200}{a_1} \tag{19}$$

$$F_3\left(M_t, a_7/a_1\right) = \frac{a_7}{a_1} - \frac{\gamma+1}{2} \frac{a_6}{a_1} + \frac{\gamma-1}{\gamma+1} \frac{M_t^2 - 1}{M_t} = 0 \tag{20}$$

$$F_4\left(M_t, a_7/a_1\right) = \gamma M_t^2 - \frac{\gamma+1}{2} \frac{p_5}{p_1} \left(\frac{a_7 / a_1}{a_5 / a_1} \right)^{2\gamma/(\gamma-1)} - \frac{\gamma-1}{2} = 0 \tag{21}$$

State 8 is given by:

$$\frac{p_8}{p_1} = \frac{2}{\gamma + 1} Y_t \tag{22}$$

$$\frac{T_8}{T_1} = \left(\frac{2}{\gamma + 1} \right)^2 \frac{X_t \, Y_t}{M_t^2} \tag{23}$$

$$\rho_1 = \frac{p_1}{R \, T_1} \tag{24}$$

$$\frac{\rho_8}{\rho_1} = \frac{\gamma+1}{2} \frac{M_t^2}{X_t} \tag{25}$$

$$M_8 = \frac{Z_t}{\left(X_t \, Y_t\right)^{1/2}} \tag{26}$$

Parameters not shown, such as M_7, are readily obtained from the above.

APPENDIX B

TABLES

Table 1. Air/air p_4 values.

M_s	p_4/p_1	p_1 Torr	p_4 bar	M_s	p_4/p_1	p_1 Torr	p_4 bar	M_s	p_4/p_1	p_1 Torr	p_4 bar	M_s	p_4/p_1	p_1 Torr	p_4 bar
2.5	145	750	145	3	631.5	750	631	3.5	3030	258	1045	4	17686	52	1219
	145	517	100		631.5	517	435		3030	103	418		17686	36	854
	145	259	50		631.5	258	218		3030	52	209		17686	26	610
	145	103	20		631.5	103	87		3030	36	146		17686	10	244
	145	52	10		631.5	52	43.5		3030	26	104		17686	5	122

Table 2. Comparative values of p_4/p_1 for driver/driven air/air and helium/air gases.

M_s	p_4/p_1	
	air/air	helium/air
2	33.67	9.664
2.5	145	21.54
3	631.5	44.16
3.5	3030	86.42
4	17686	165.2

Table 3. Shock tube parameters (for driver/driven - air/air) with a 13.65 area contraction.
[γ = 1.4, R = 287 J/kg-K, T_1 = 300 K]

M_s	M_t	M_2	M_8	p_1 Torr	p_4 bar	p_4/p_1	p_2/p_1	p_2 bar	p_8/p_1	p_8 bar	T_2 K	T_8 K	w_2 m/s	w_8 m/s
2.5	2.96	1.20	1.35	750	145	145	7.13	7.20	10.07	10.1	641	790	608	759
2.6	3.08	1.23	1.38	750	194	194	7.72	7.72	10.92	10.9	672	833	641	798
2.7	3.20	1.27	1.41	595	206	260	8.34	6.61	11.81	9.36	703	878	674	837
2.8	3.33	1.30	1.44	440	204	349	8.98	5.26	12.73	7.46	735	924	707	875
2.9	3.45	1.33	1.46	336	210	469	9.65	4.32	13.69	6.14	769	973	739	913
3	3.57	1.36	1.48	259	218	633	10.33	3.56	14.68	5.06	804	1022	772	951
3.1	3.69	1.38	1.51	181	207	857	11.05	2.66	15.71	3.79	840	1074	804	989
3.2	3.81	1.41	1.53	129	201	1165	11.78	2.03	16.77	0.20	877	1127	835	1026
3.3	3.93	1.43	1.54	103	220	1594	12.54	1.73	17.86	2.46	915	1182	867	1064
3.4	4.05	1.45	1.56	77.6	227	2193	13.32	1.38	18.99	1.96	954	1239	899	1101
3.5	4.17	1.47	1.58	51.7	209	3037	14.13	0.97	20.16	1.39	995	1297	930	1138
3.6	4.29	1.49	1.59	36.2	205	4240	14.95	0.72	21.35	1.03	1036	1357	961	1175
3.7	4.42	1.51	1.61	25.9	206	5970	15.81	0.55	22.59	0.78	1079	1419	992	1212
3.8	4.54	1.52	1.62	18.1	205	8488	16.68	0.40	23.85	0.57	1123	1482	1023	1249
3.9	4.66	1.54	1.63	12.9	210	12198	17.58	0.30	25.16	0.43	1168	1548	1054	1286
4	4.78	1.55	1.64	8.79	208	17740	18.50	0.21	26.49	0.31	1214	1614	1085	1323

Table 4. Bench test results with a negative corona.

Discharge voltage kV	Discharge current without airflow μA	Discharge current with airflow μA	Ring probe output (amplifier gain =10^2) without airflow V_{rms}	Ring probe output (amplifier gain =10^2) with airflow V_{rms}
0	0	0	0.0161	0
1	0	0	0.0182	0
2	0	0	0.0203	0
3	0	0	0.0196	0
4	0	0	0.0218	0.0202
5	0.5	0.5	0.0217	0.0211
6	0.5	0.5	0.0203	0.0218
7	0.5	0.5	0.0323	0.025
7.5	1	0.75	0.0213	0.0213
7.75	1	0.75	0.0803	0.0247
8	4	3	0.134	0.291
8.25	8	4	0.241	0.414
8.5	11	6	0.352	0.521
8.75	15	9	0.421	0.605
9	19	12	0.514	0.756
9.25	23	14	0.76	0.736
9.5	24	15	0.73	0.706

Table 5. Bench test results with a positive corona,
(a) without amplifier in the probe circuit, (b) with amplifier in the probe circuit.

(a)

Discharge voltage	Discharge current		Ring probe output (without amplifier)	
	without airflow	with airflow	without airflow	with airflow
kV	μA	μA	V_{rms}	V_{rms}
4	0	0	0	0
5	0	0	0	0
6	0	0	0	0
7	0	0	0	0
8	0	0	0	0
8.25	0	0	0	0
8.5	0	0	0	0
8.75	0	0	0	0
9	3	2	0.156	0.064
9.25	15	12	0.314	0.392
9.5	40	30	0.561	0.611

(b)

Discharge voltage	Discharge current		Ring probe output (amplifier gain $=10^2$)	
	without airflow	with airflow	without airflow	with airflow
kV	μA	μA	V_{rms}	V_{rms}
4	0	0	0	0
5	0	0	0	0
6	0	0	0	0
7	0	0	0.024	0
8	0	0	0.022	0
8.25	0	0	0.024	0
8.5	0	0	0.0227	0.0227
8.75	0	0	0.0228	0.0224
9	3	2	0.672	0.568
9.25	15	12	4.61	4.487
9.5	40	30	4.361	4.296

Table 6. List of shock tube runs, $p_1 = 10^2$ kPa.

Run	Date	p_4 MPa (psi)	Corona discharge	Type of flow
1	02/19/05	0.1 (14.5)	Negative 0-9.55 kV	Quiescent (static air)
2	02/21/05	1.38 (200)	Negative 9 kV	Subsonic
3	02/28/05	1.38 (200)	Negative 9 kV	Subsonic
4	03/07/05	1.24 (180)	Negative 8.66 kV	Subsonic
5	03/11/05	1.31 (190)	Negative 9 kV	Subsonic
6	03/16/05	1.28 (185)	Negative 9 kV	Subsonic
7	03/17/05	13 (1900)	Negative 9 kV	Supersonic
8	03/18/05	15 (2195)	Negative 8 kV	Supersonic
9	03/22/05	14.5 (2100)	Negative 8.55 kV	Supersonic
10	03/23/05	14.5 (2100)	No corona	Supersonic
11	03/28/05	14.5 (2100)	No corona	Supersonic
12	03/29/05	14.5 (2100)	Negative 9.55 kV	Supersonic
13	03/30/05	0.1 (14.5)	Negative 9.55 kV	Quiescent (static air)
14	04/01/05	1.31 (190)	No corona	Subsonic

Table 7 Data uncertainty

Measured variables	Uncertainty
ΔL	± 0.001 m
Δt	± 0.013 x 10^{-3} s
T_1	± 1 K
p_2	± 2 %
V	± 1 %
I	± 2 %
V_{rms}	± 1.3 %

APPENDIX C

FIGURES

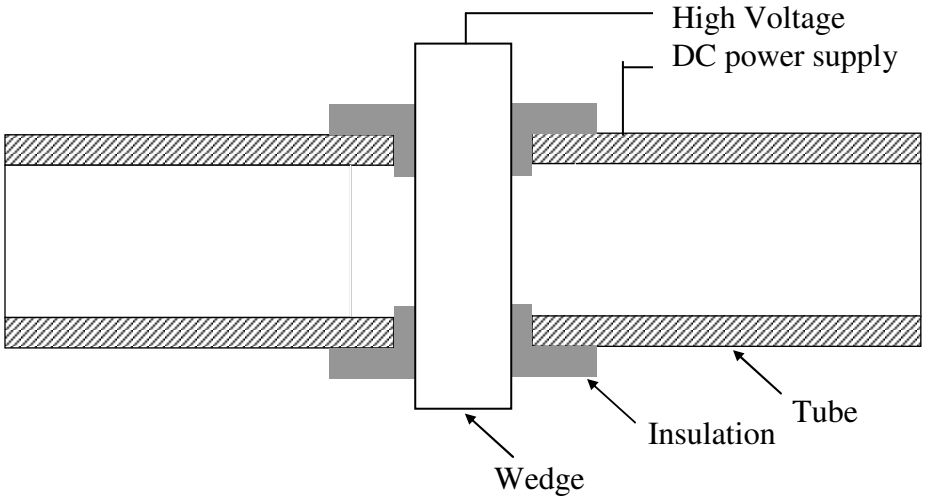

(a)

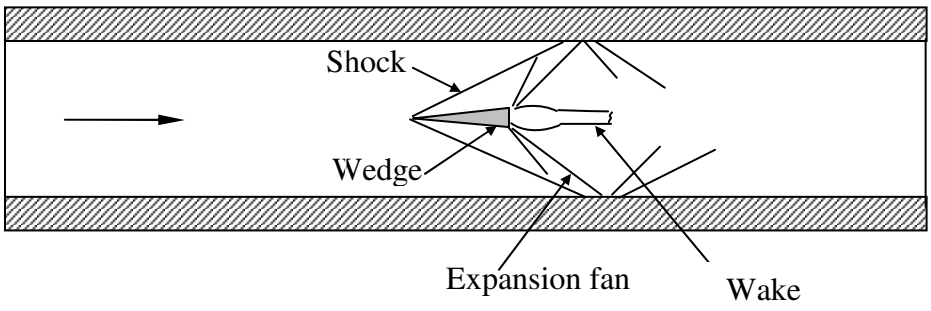

(b)

Figure 1. Schematic of device for generating a corona in a supersonic flow, (a) Side view, (b) Top view.

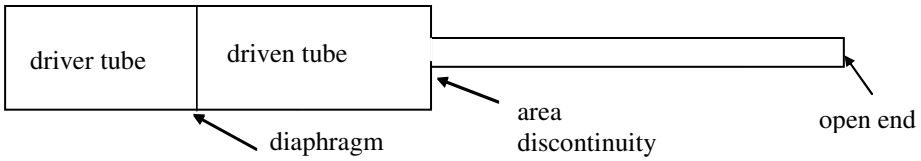

(a)

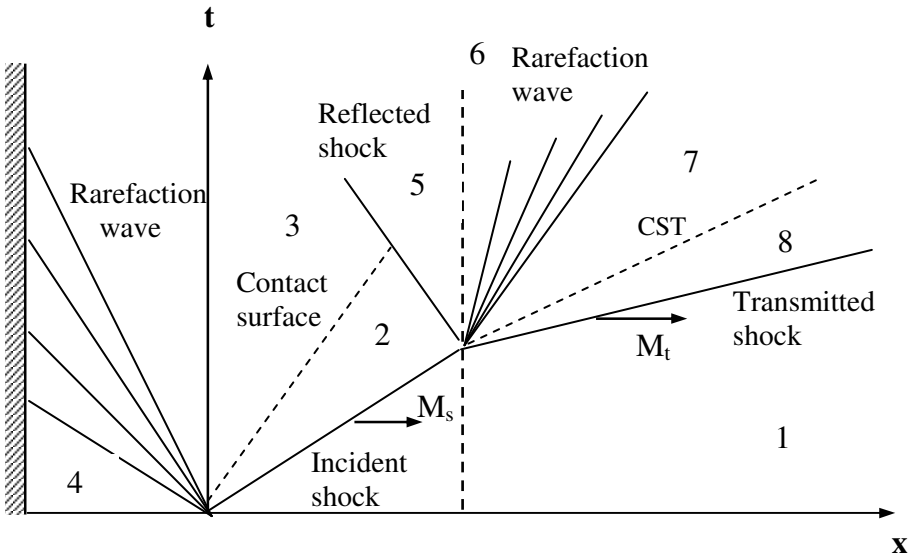

(b)

Figure 2. Configuration and wave diagram for a shock tube with an area contraction in the driven section,
(a) Schematic, (b) Idealized wave diagram.

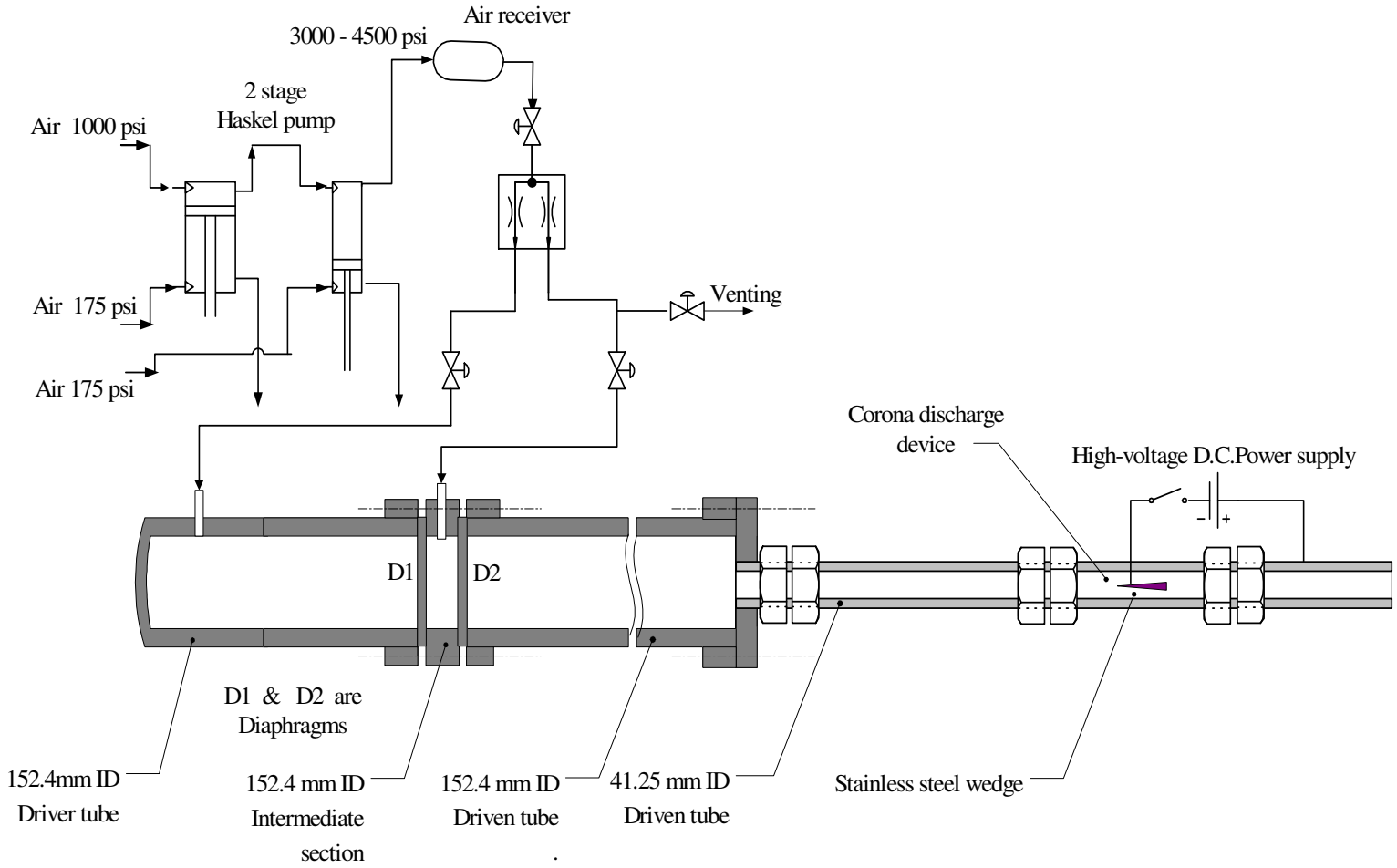

Figure 3. Layout (schematic) of the shock tube for a corona discharge in supersonic air.

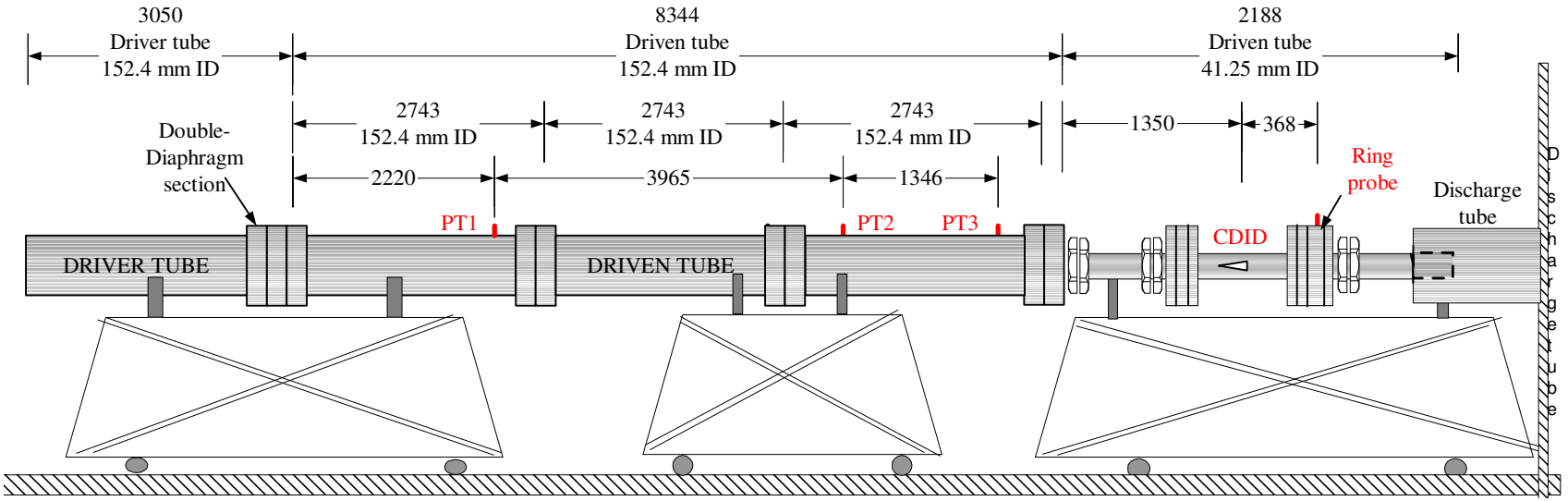

CDID – Corona Discharge Ionization Device
PT1 - Triggering pressure transducer
PT2 and PT3 - Pressure Probes
Ring Probe - Plasma Probe

Figure 4. Layout of the shock tube with the CDID and instrumentation (dimensions in mm).

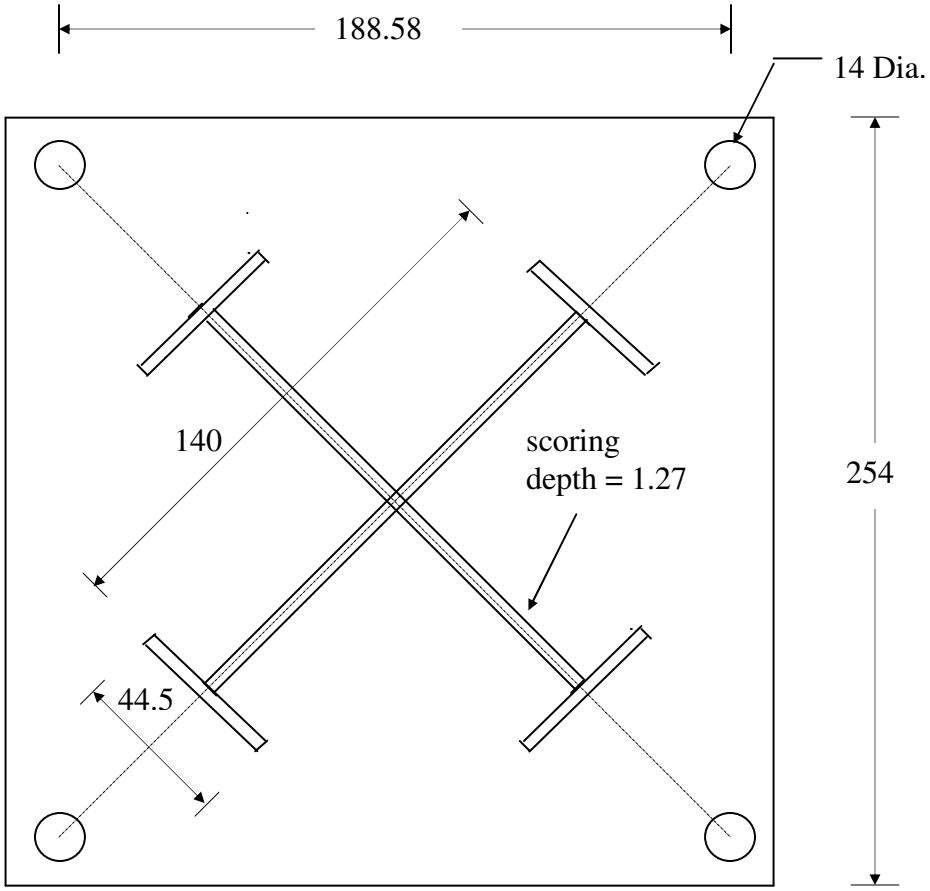

Figure 5. Diaphragm (dimensions in mm).

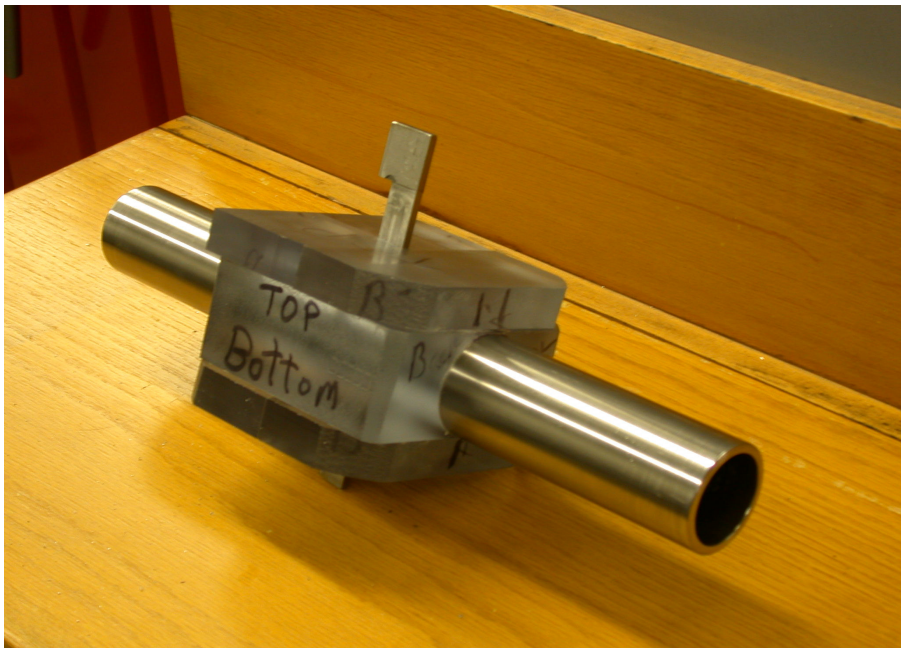

(a)

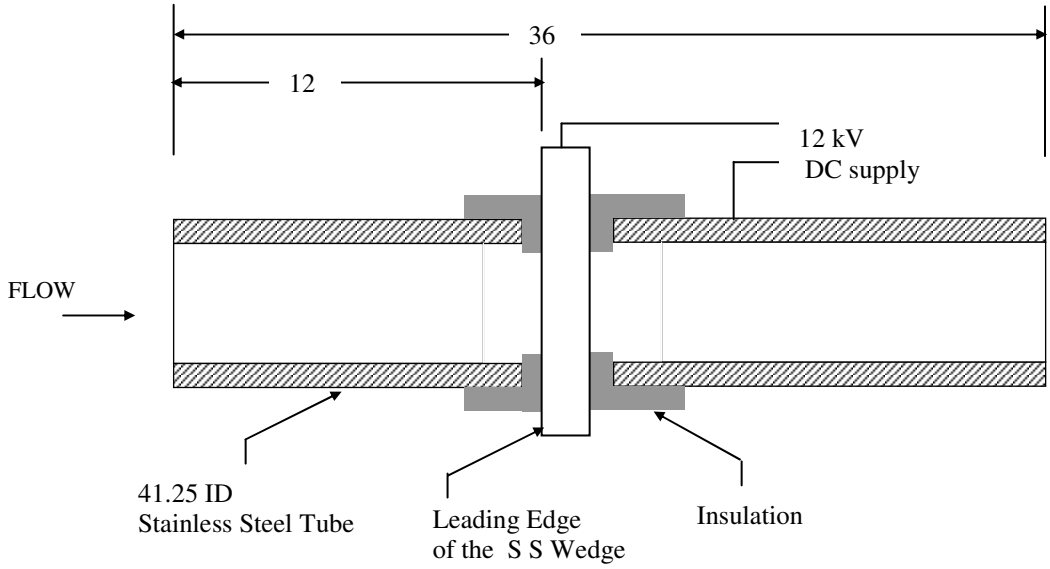

(b

Figure 6. Corona discharge ionization device (CDID) (dimensions in mm), (a) Photograph, (b) Schematic.

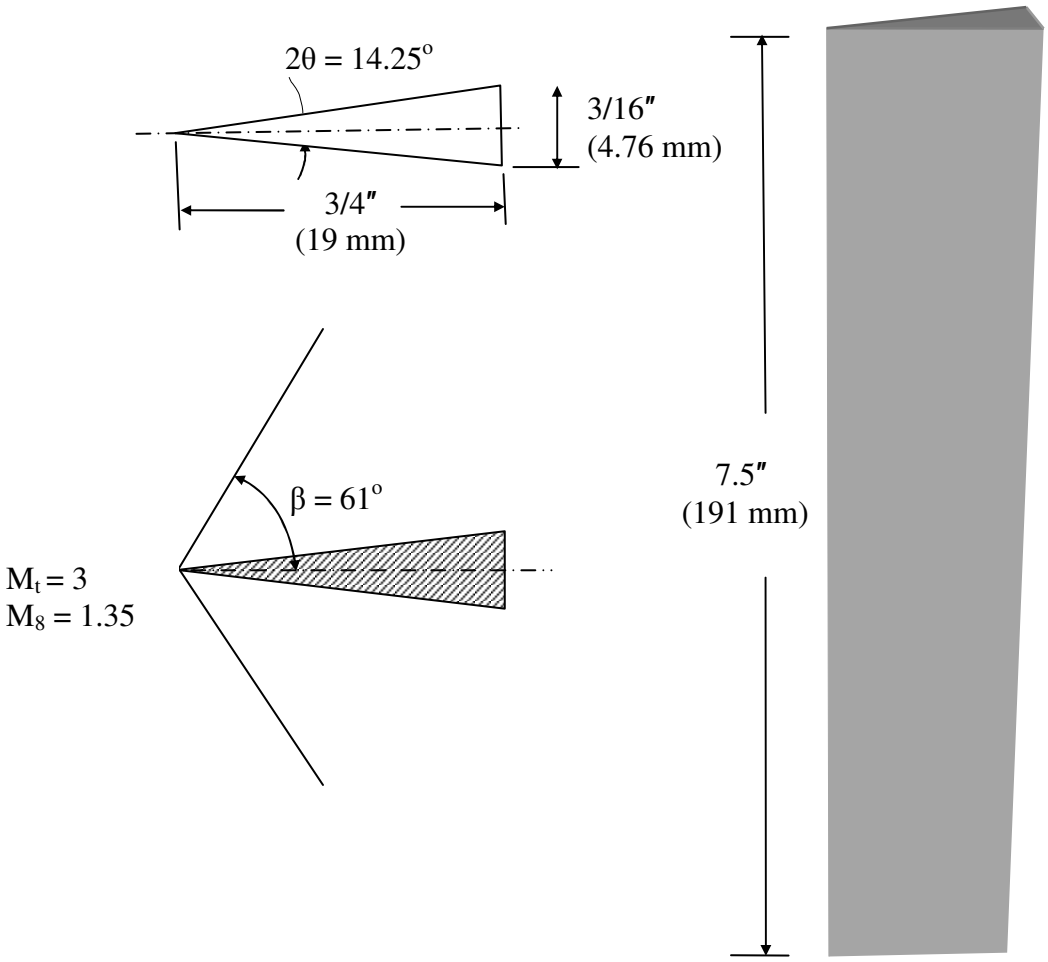

Figure 7. Wedge electrode geometry.

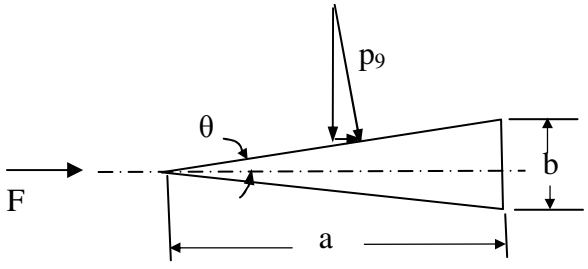

Figure 8. Pressure loading diagram.

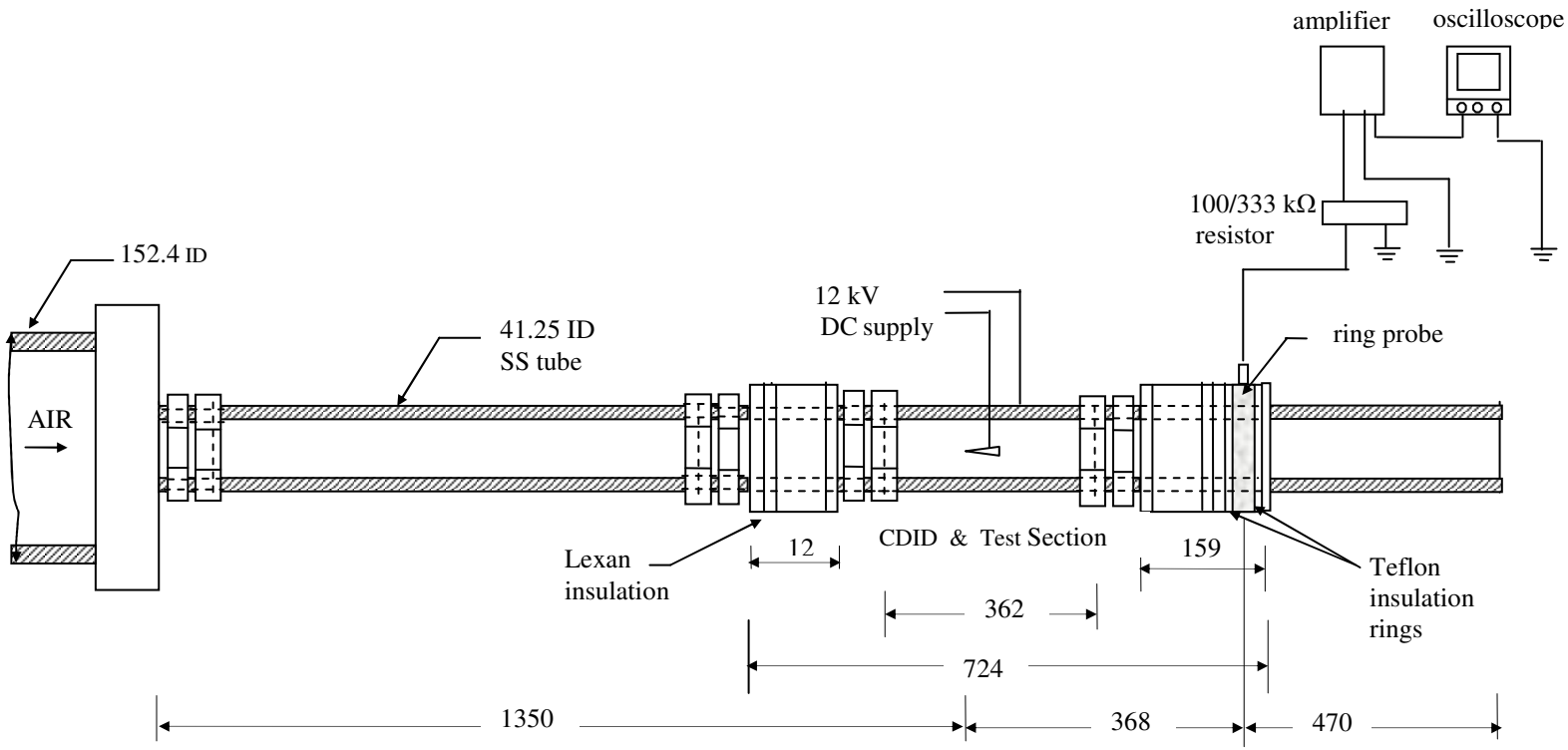

Figure 9. Schematic layout of the CDID and the test section in the shock tube (dimensions in mm).

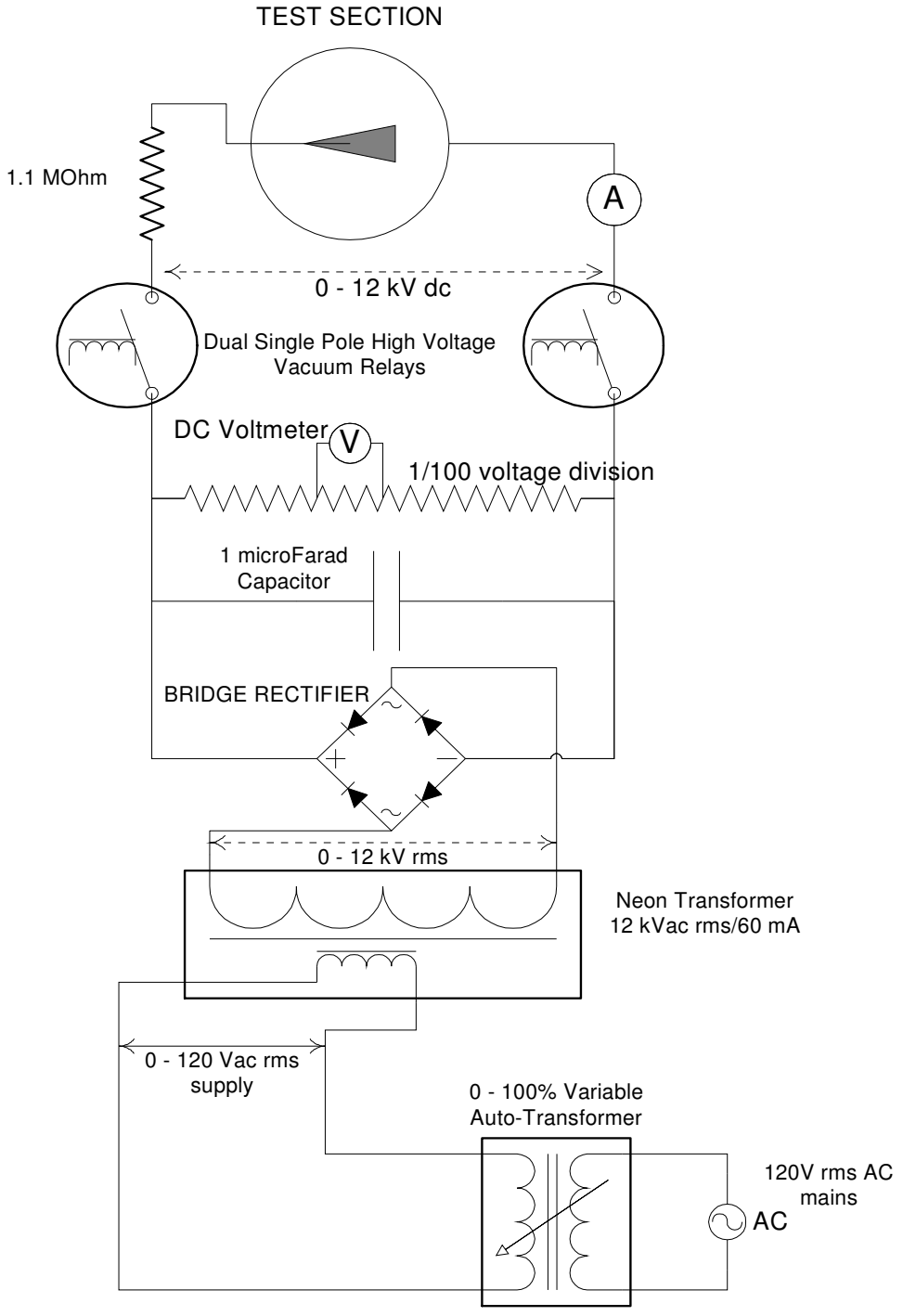

Figure 10. DC power supply unit

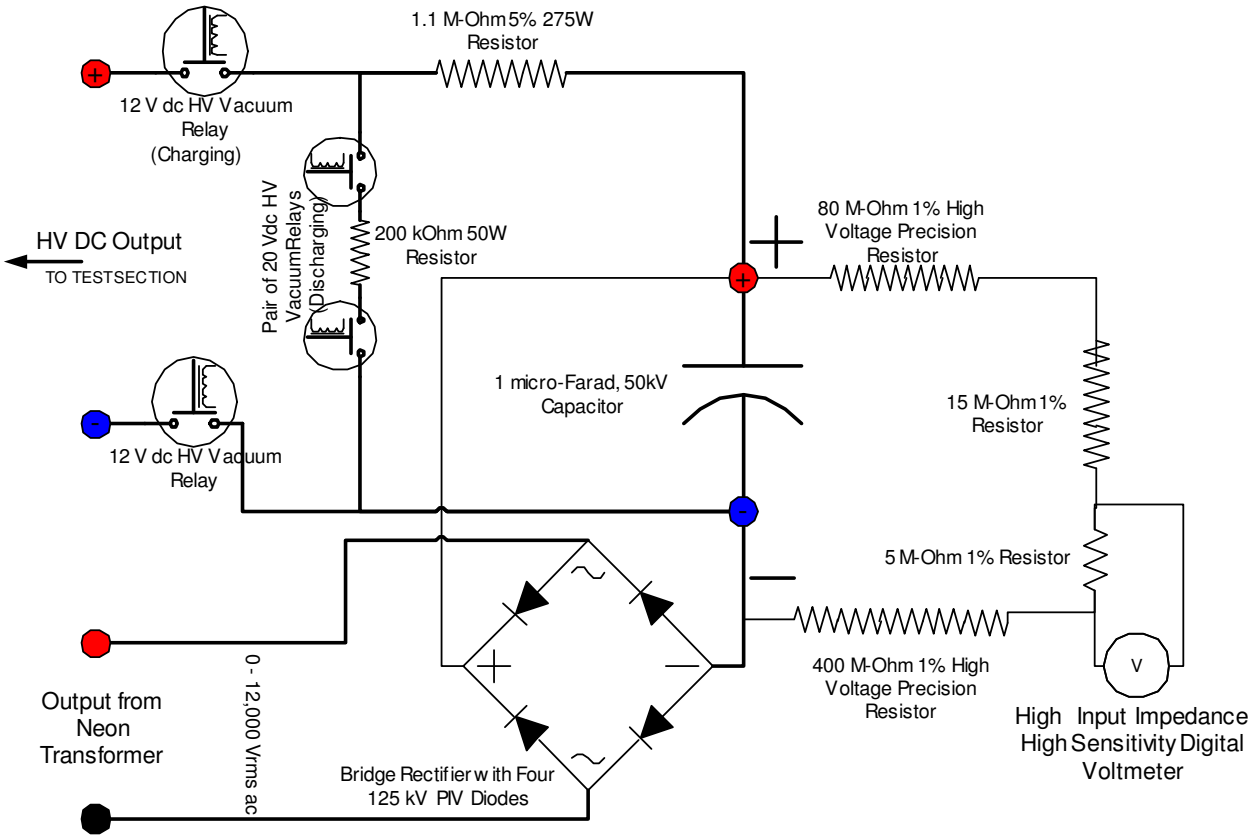

Figure 11. Relays and digital voltmeter in the DC power supply circuit.

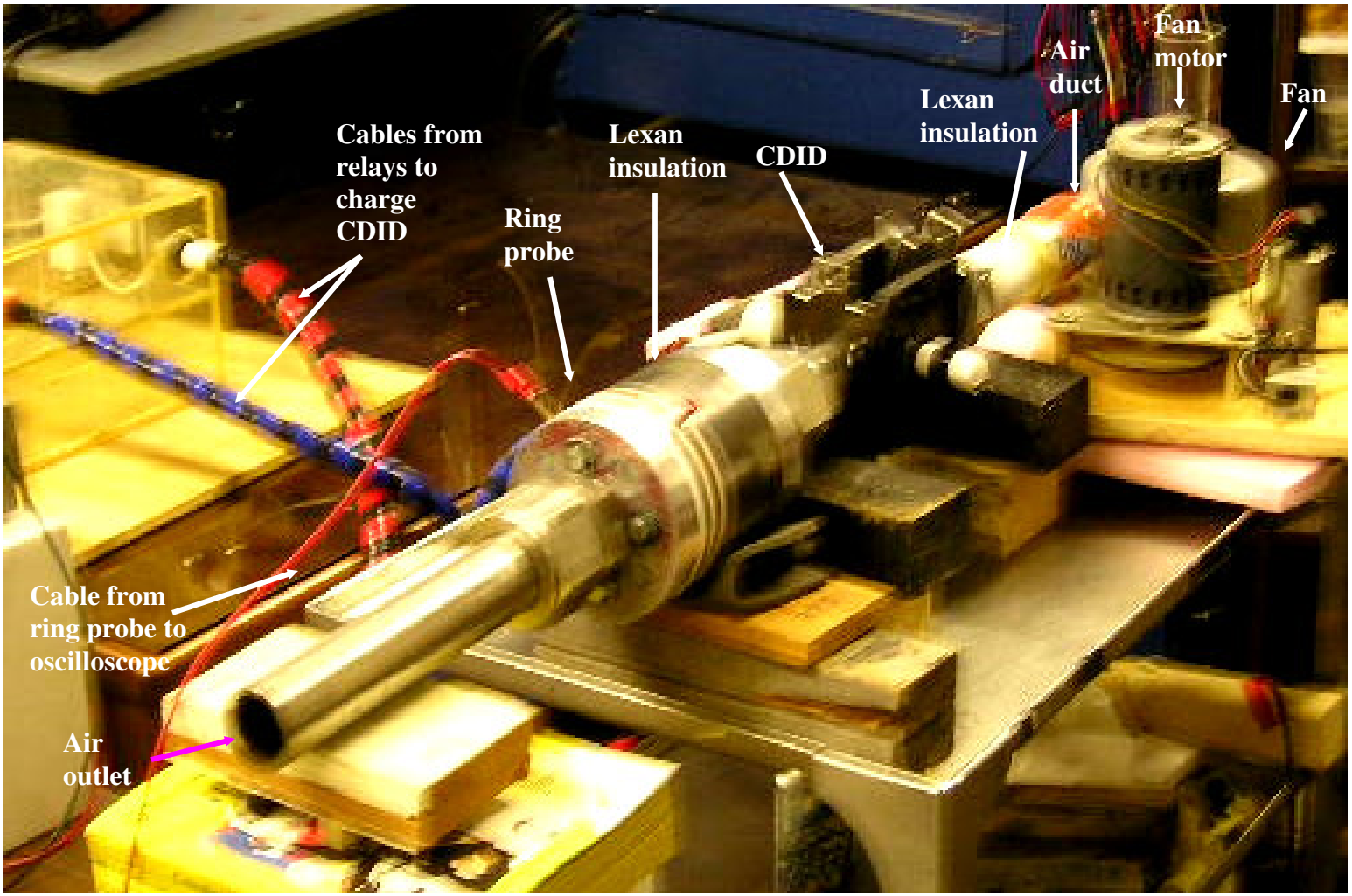

Figure 12. Bench test layout.

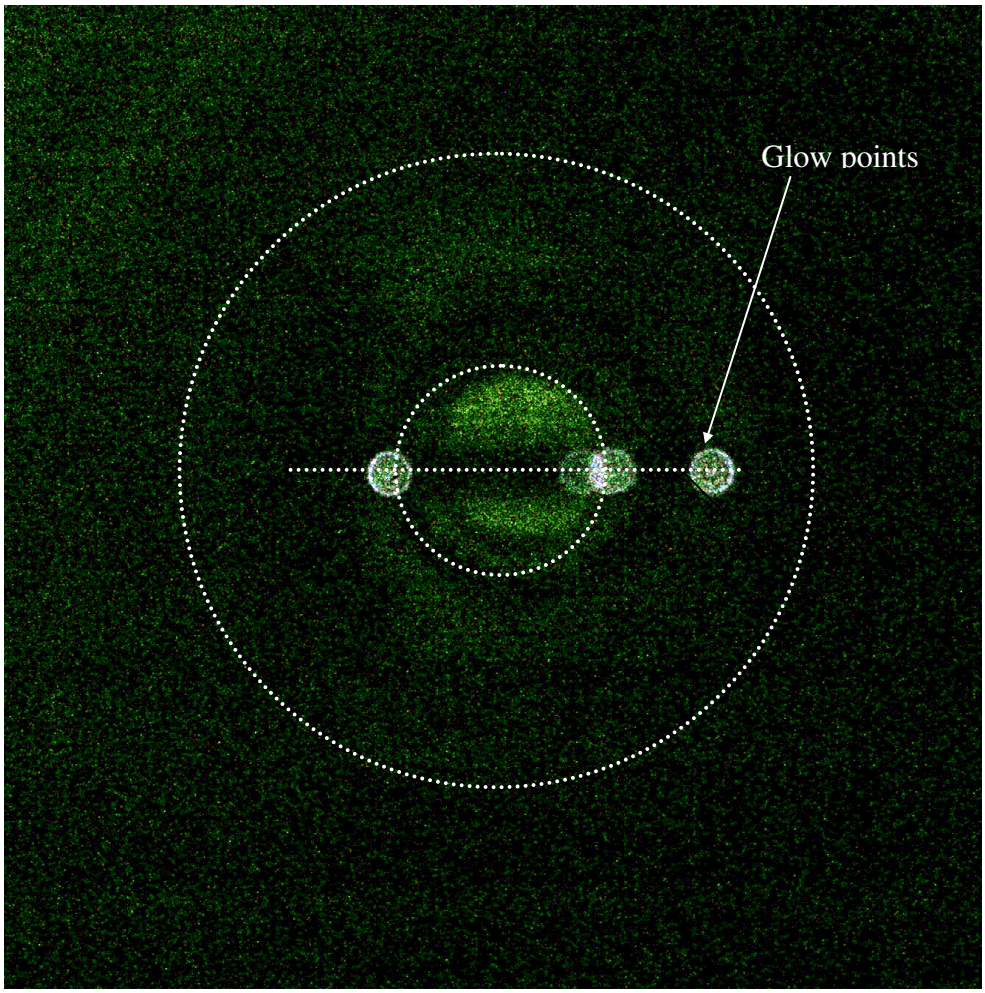

Figure 13. Corona glow points along the leading edge of the wedge. Dotted lines are drawn to indicate the location of the leading edge and to represent the inner upstream and downstream ends of the CDID.

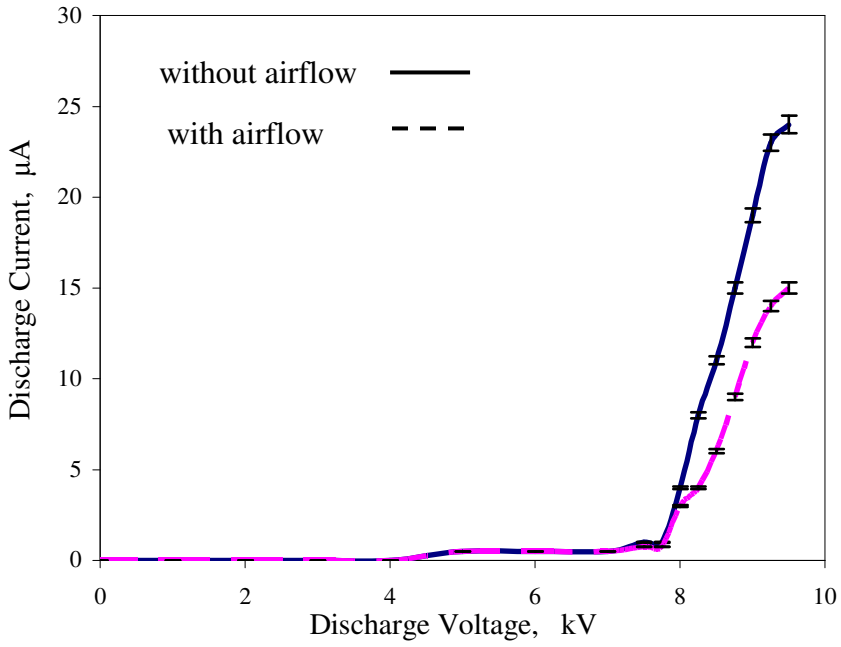

(a)

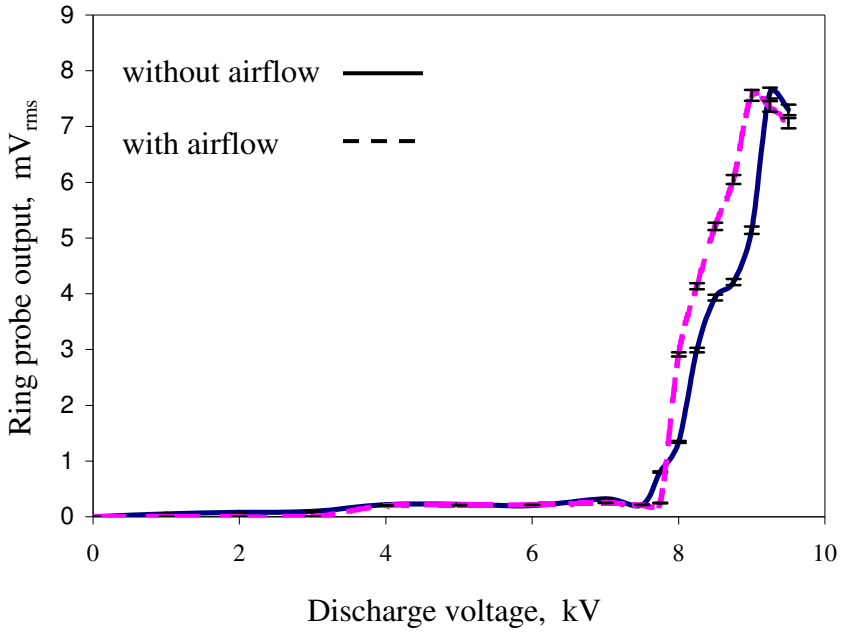

(b)

Figure 14. Bench test results with a negative corona,
(a) Corona discharge characteristic, (b) Probe characteristic.

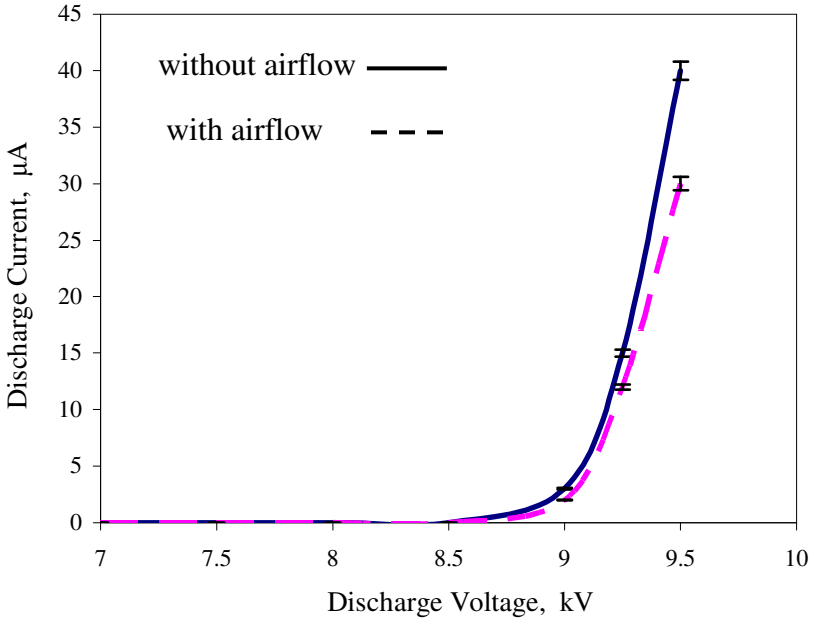

(a)

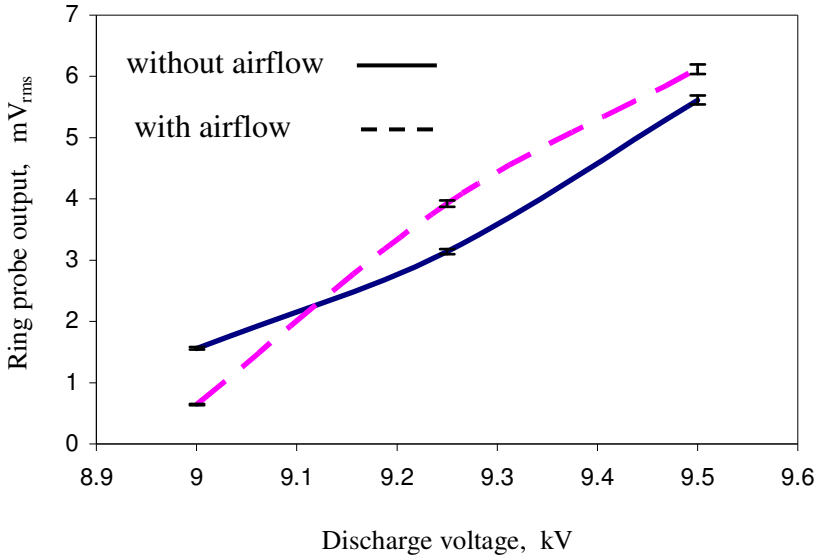

(b)

Figure 15. Bench test results with a positive corona,
(a) Corona discharge characteristic, (b) Probe characteristic.

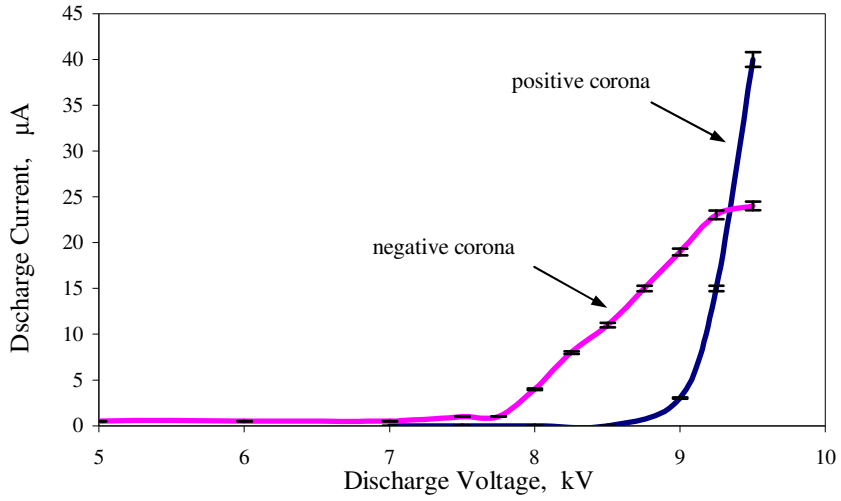

(a) .

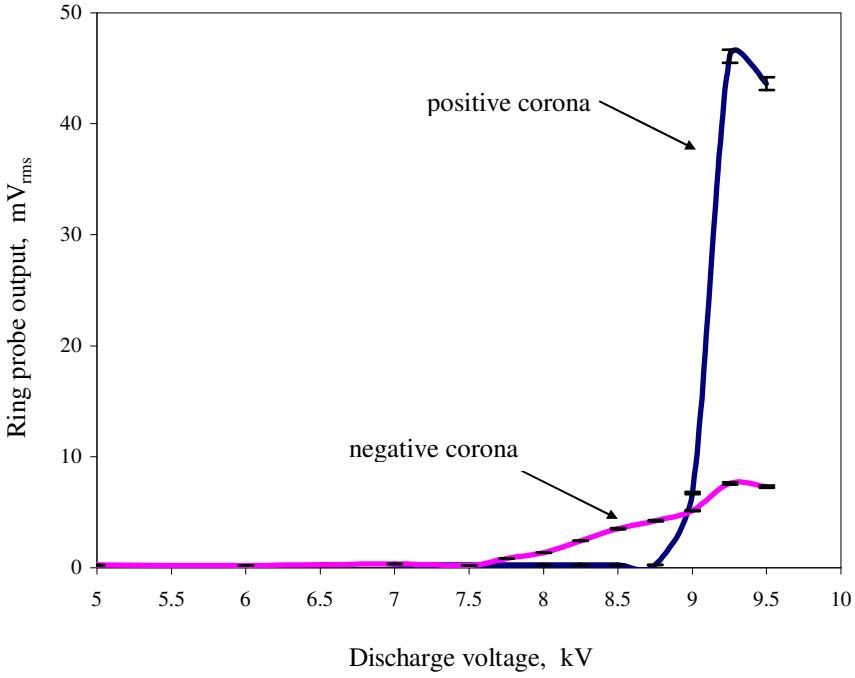

(b)

Figure 16. Bench test results with positive and negative coronas, (a) Discharge characteristics, (b) Probe characteristics.

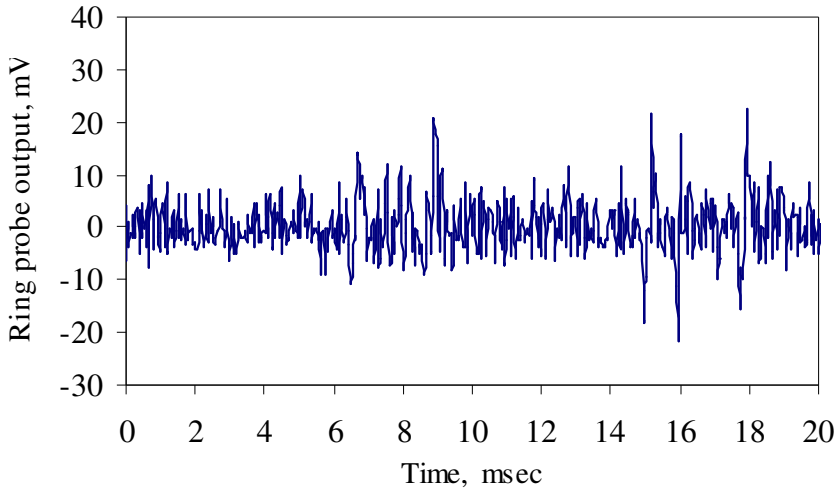

(a)

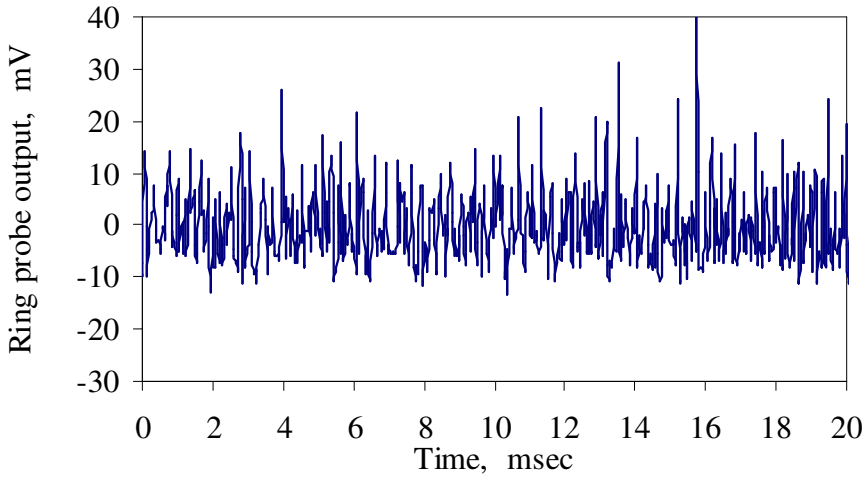

(b)

Figure 17. Bench test results – probe output of a negative corona at 9 kV, (a) in static air, V_{rms} = 5.14 mV, (b) with airflow from a fan, V_{rms} = 7.56 mV.

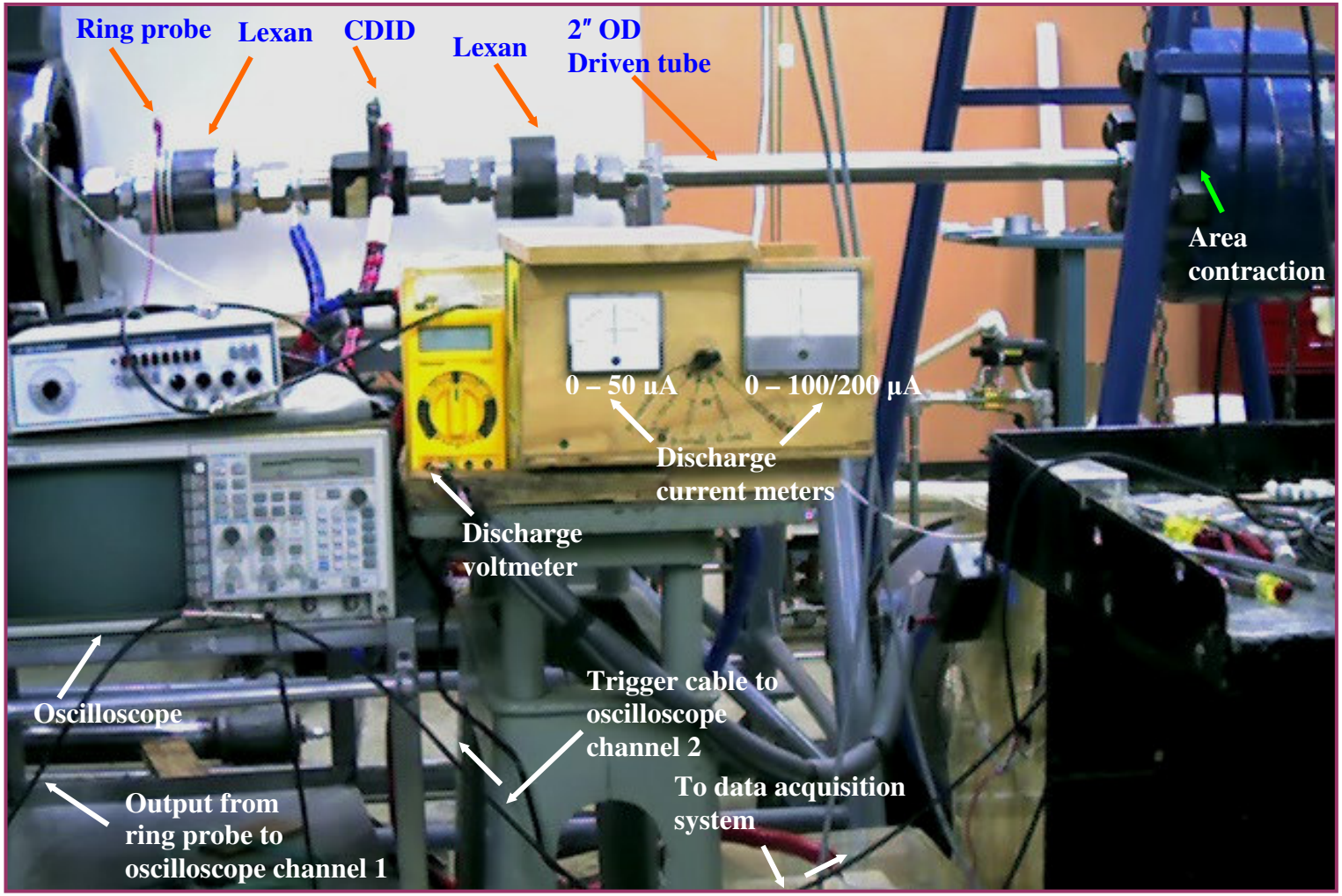

Figure 18. Labelled photograph showing part of the shock tube with the CDID installed and instrumentation.

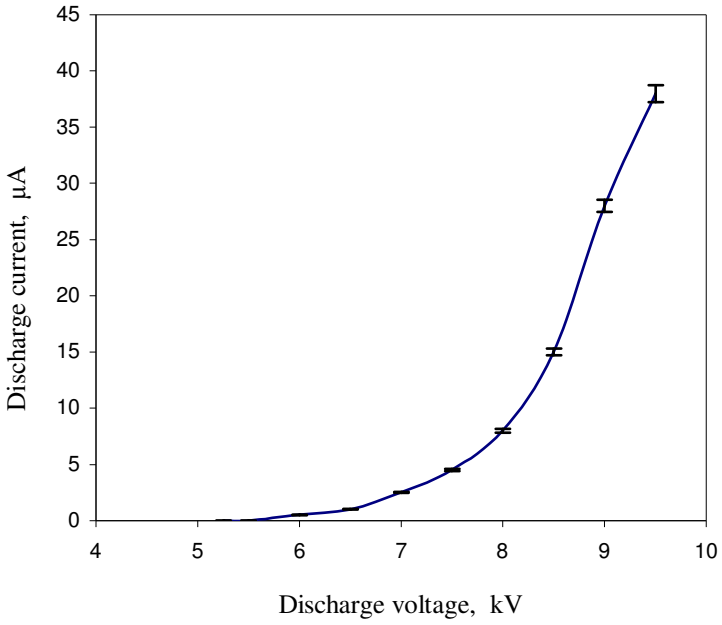

(a)

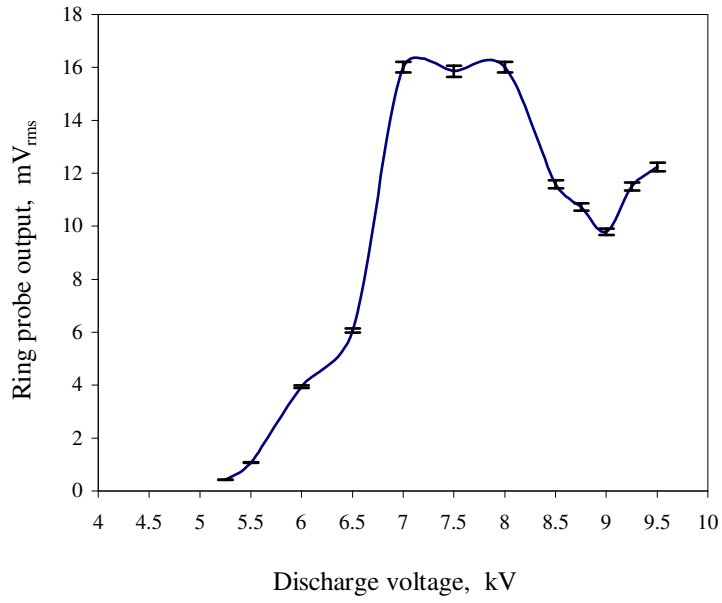

(b)

Figure 19. Static test on CDID in the shock tube with a negative corona (Run 1), (a) Discharge current versus discharge voltage, (b) Ring probe output versus discharge voltage.

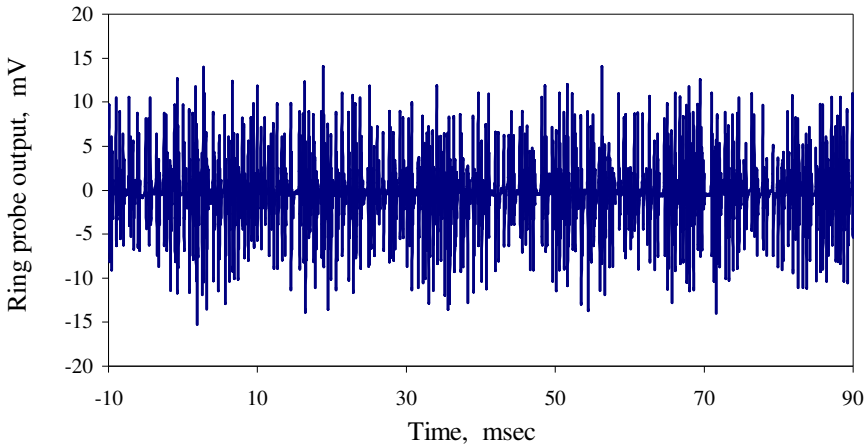

(a)

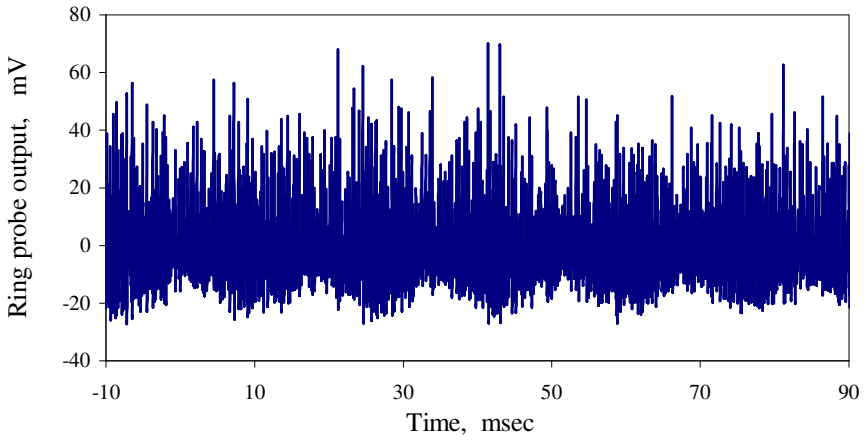

(b)

Figure 20. Sample outputs from static test on CDID in the shock tube (Run 1). (a) Pulsed output for a discharge voltage 6 kV, (b) Pulsed output for a discharge voltage of 8 kV.

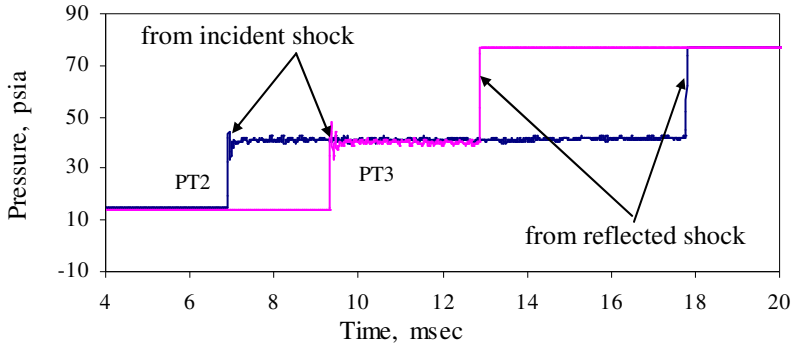

(a)

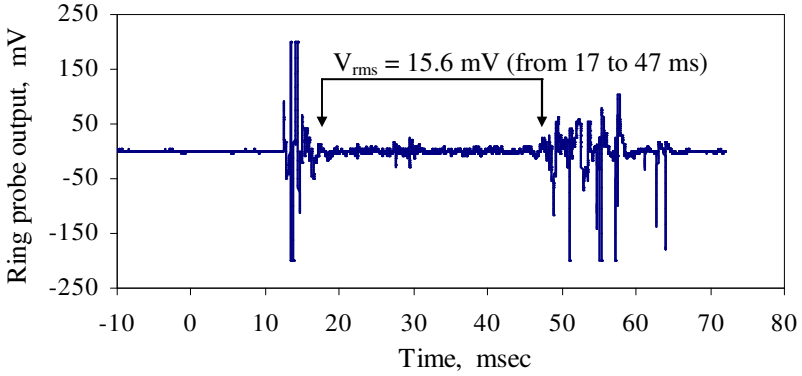

(b)

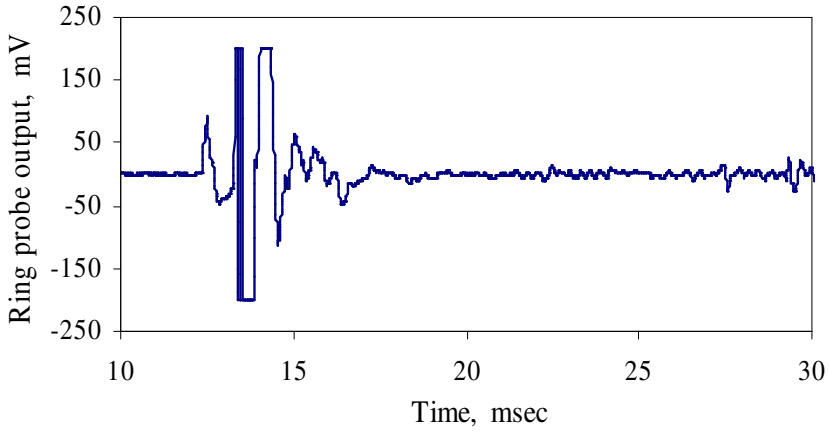

(c)

Figure 21. Results for subsonic flow with a negative corona at 9 kV (Run 6), (a) Data from the pressure transducers PT2 and PT3, (b) Data from the ring probe, (c) Data from the ring probe (expanded).

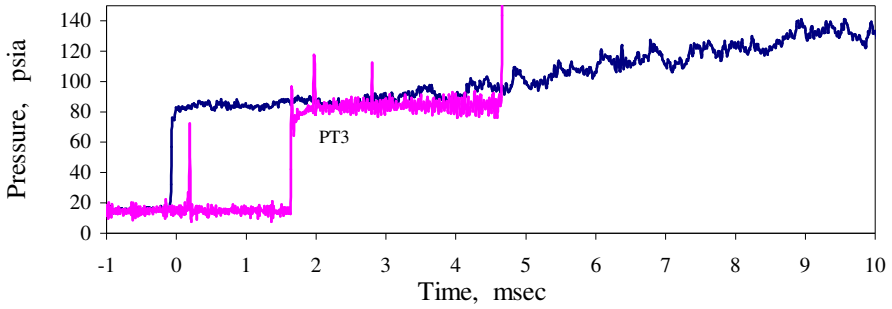

(a)

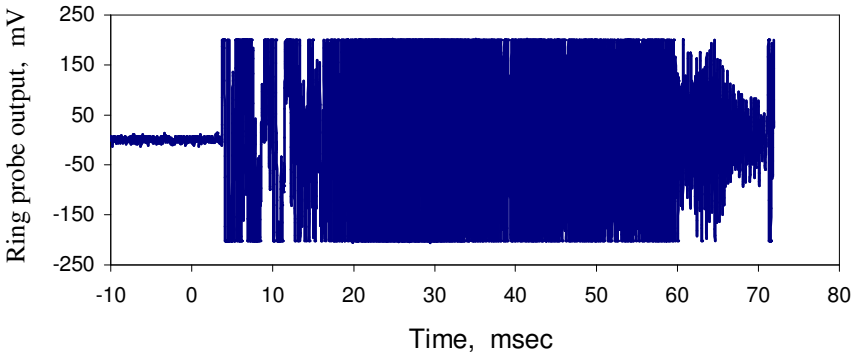

(b)

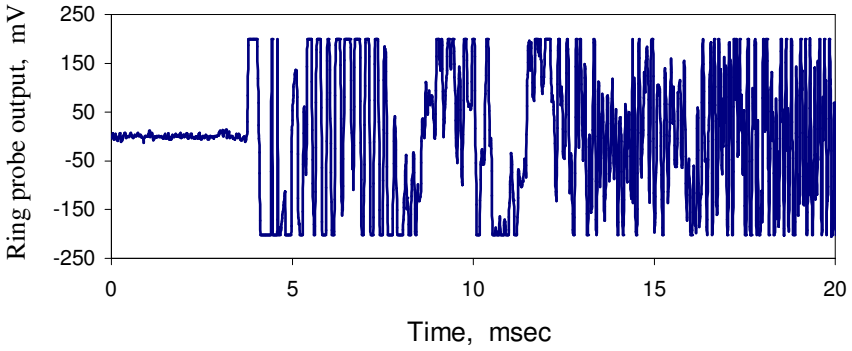

(c)

Figure 22. Results for supersonic flow with a negative corona at 8.55 kV (Run 9), (a) Data from the pressure transducers, (b) Pulsed output for a corona at 8.55kV, (c) Pulsed output for a corona at 8.55 kV (expanded).

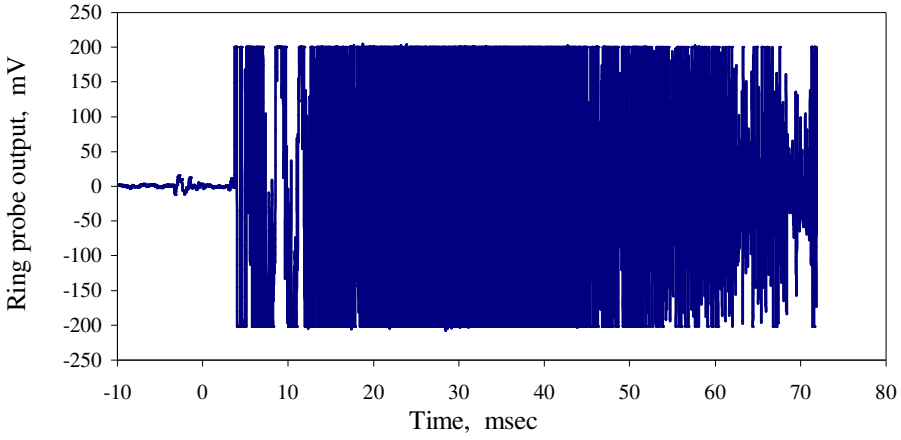

Figure 23. Result for supersonic flow without a corona (Run 10).

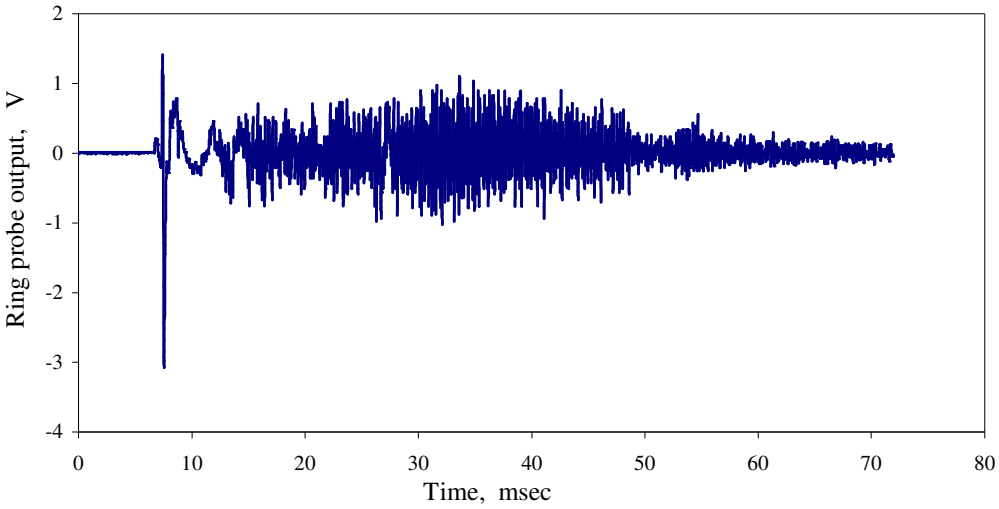

(a)

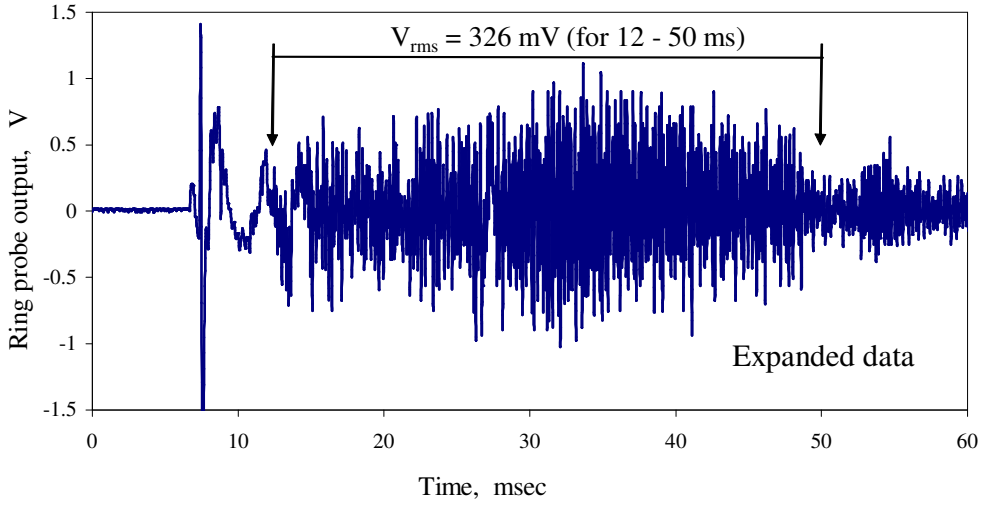

(b)

Figure 24. Result for supersonic flow with a negative corona at 9.55 kV (Run 12), (a) Ring probe output, (b) Ring probe output (expanded data).

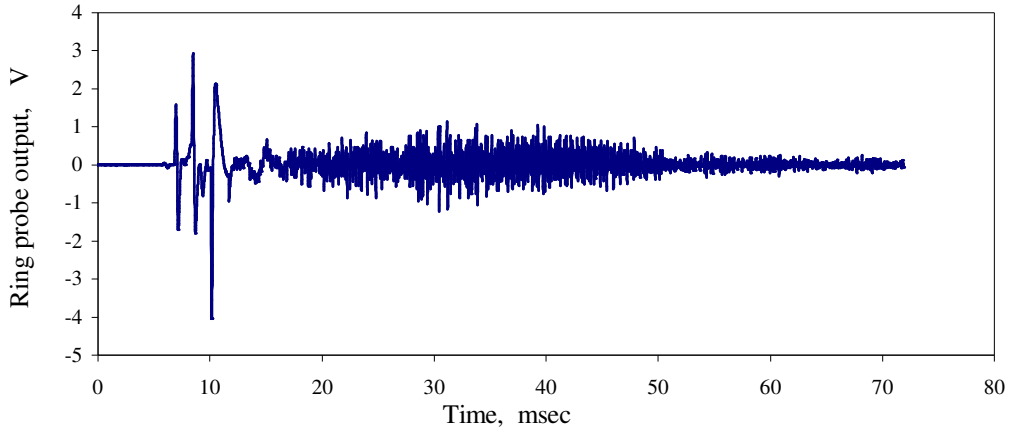

(a)

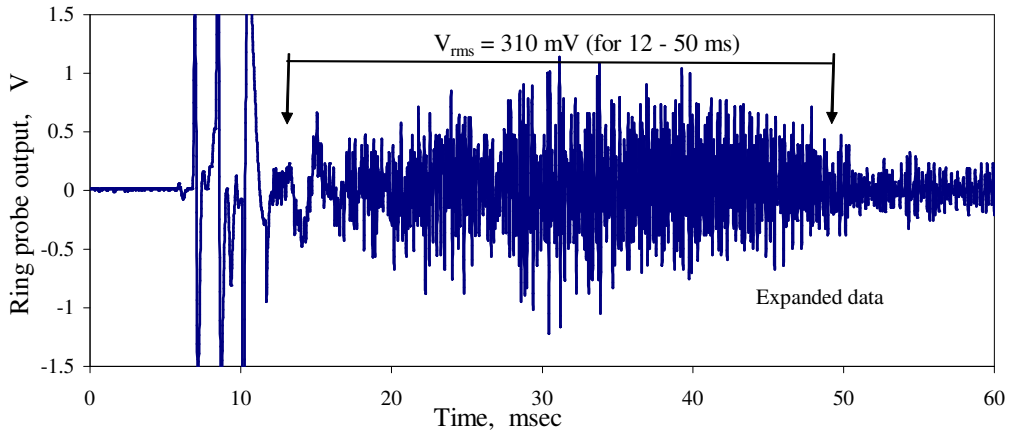

(b)

Figure 25. Result for supersonic flow without a corona (Run 11), (a) Ring probe output, (b) Ring probe output (expanded data).

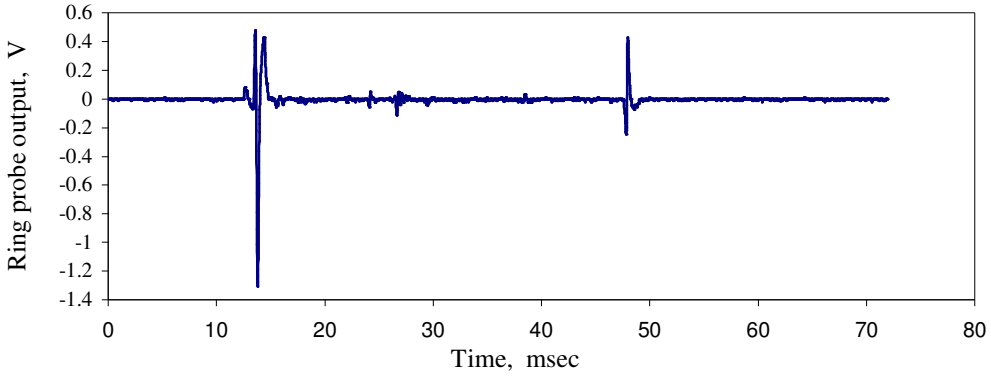

(a)

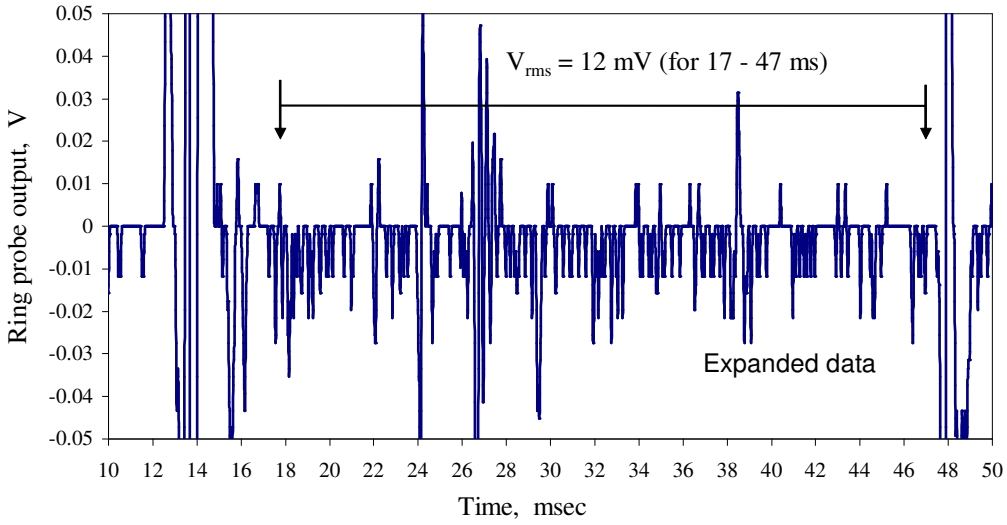

(b)

Figure 26. Result for subsonic flow without a corona (Run 14), (a) Ring probe output, (b) Ring probe output (expanded data).

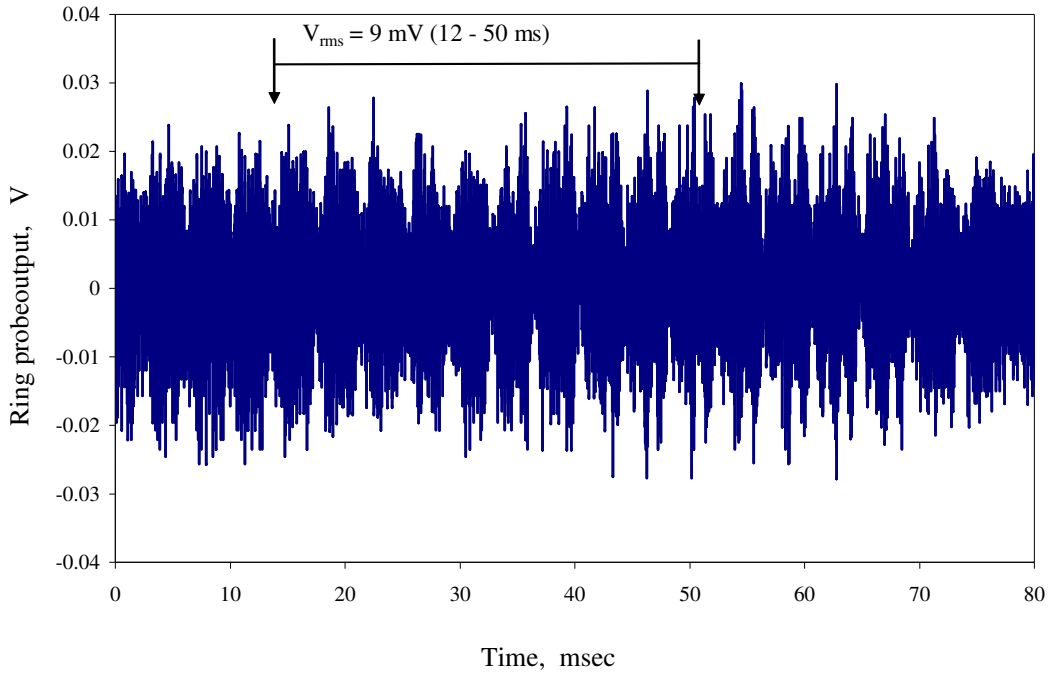

Figure 27. Result from a static test in ambient air with a negative corona at 9.55 kV (Run 13).

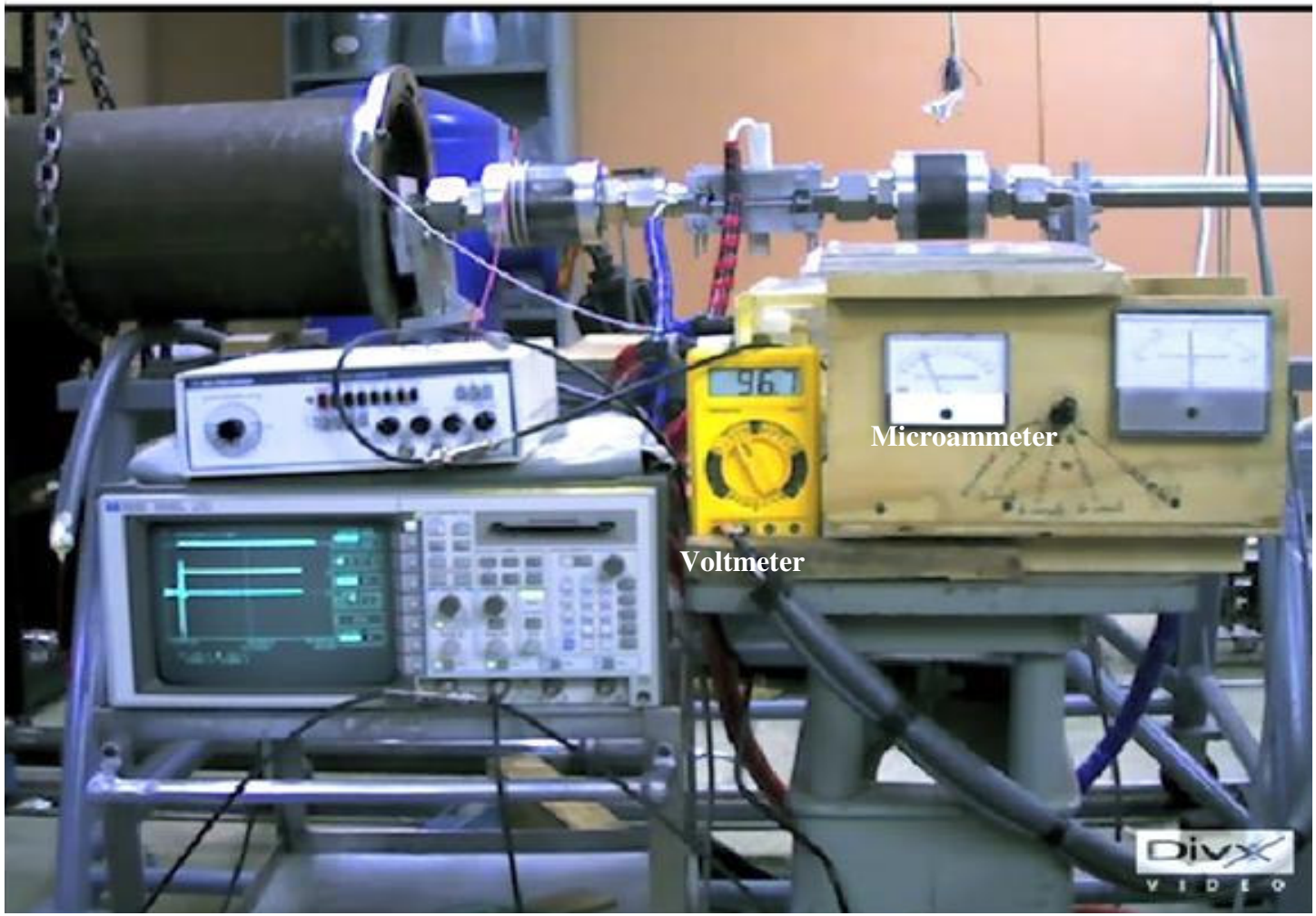

Figure 28. Oscilloscope image of the output signal before the diaphragm rupture (Run 12).

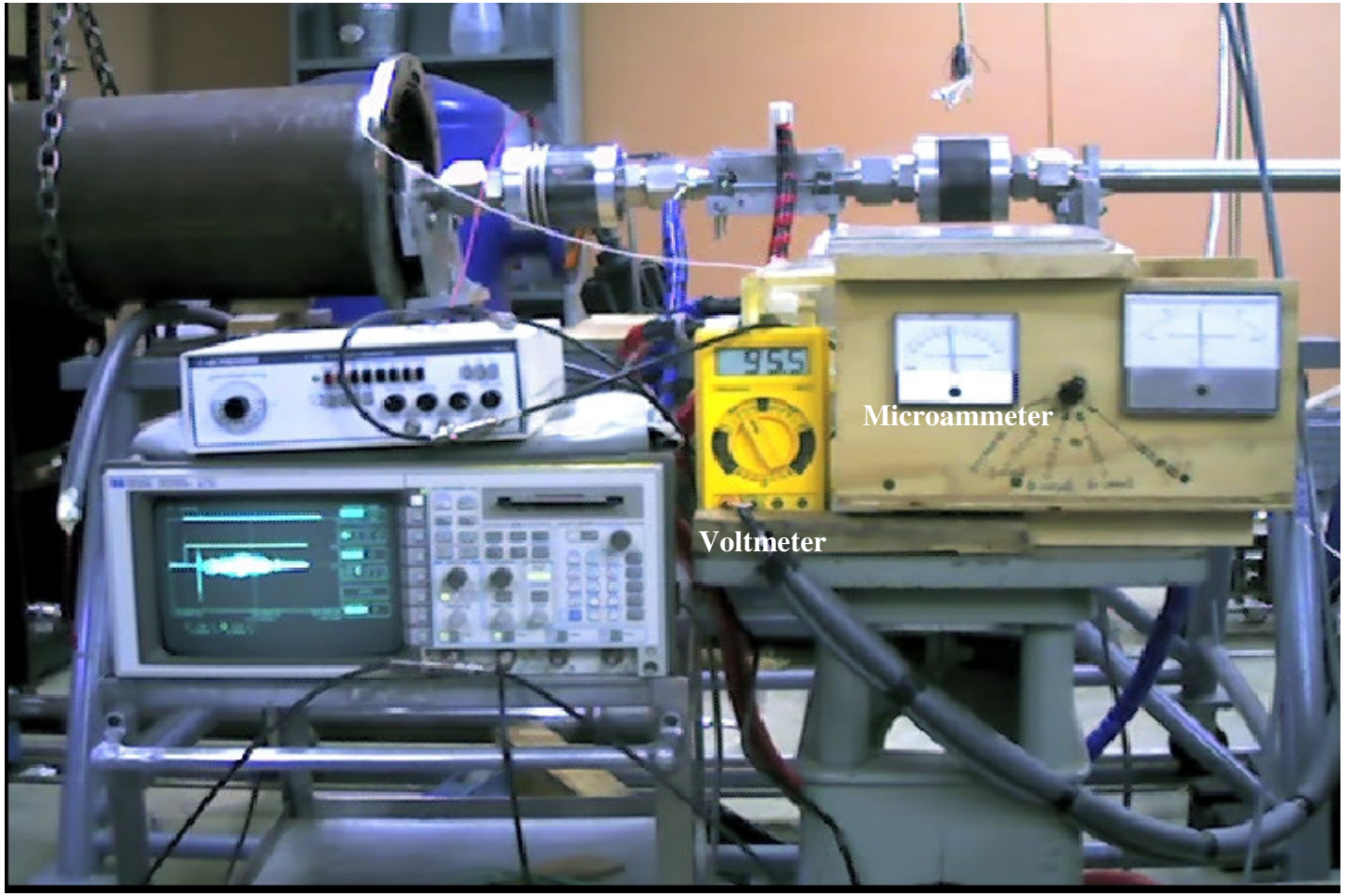

Figure 29. Oscilloscope image of the output signal right after the diaphragm rupture (Run 12).

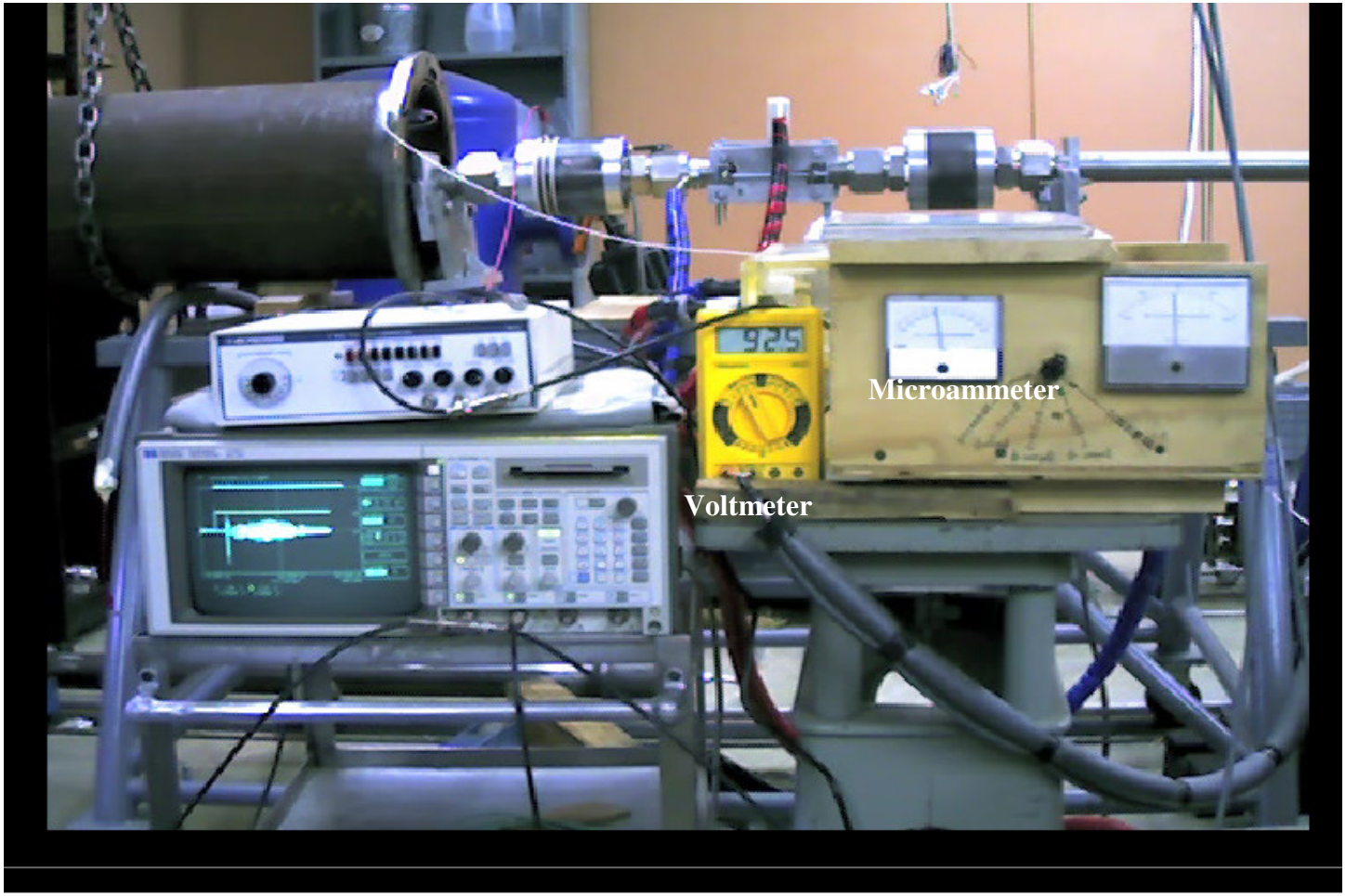

Figure 30. Oscilloscope image of the output signal a little after the diaphragm rupture (Run 12).

REFERENCES

1. Howatson, A. M., *Introduction to Gas Discharges*, 2nd ed., Pergamon Press, New York, 1976, p. 71.
2. Rich, J. W., Bergman, R. C., and Lordi, J. A., "Electrically Excited, Supersonic Flow Carbon Monoxide Laser," *AIAA Journal*, Vol. 13, No. 1, 1975, pp. 95-101.
3. Liu, H. C., Stussey, W. S., Lu, F. K., and Wilson, D. R., "Design of an Electrical Conductivity Channel for Shock Tunnel," AIAA Paper 1996-2198, 1996.
4. Slavin, V. S., Gavrilov, V. M., Zelinsky, N. L., and Bozhkov, A. R., "Magnetohydrodynamic Generator with Plasma Layers as Power Source Aboard a Hypersonic Airplane," *Journal of Propulsion and Power*, Vol. 17, No. 1, 2001, pp. 19-26.
5. Stussey, W. S., Lu, F. K., and Wilson, D. R., "Shock-Induced Detonation Wave Driver For Enhancing Shock Tube performance," AIAA Paper 1998-0549, 1998.
6. Macheret, S. O., Shneider, M. N., Miles, R. B., and Lipinski, R. J., "Electron-Beam-Generated Plasmas in Hypersonic Magneto-hydrodynamic Channels," *AIAA Journal*, Vol. 39, No. 6, 200, pp. 1127-1138.

7. Palm, P., Plonjes, E., Buoni, M., Subramaniam, V. V., Adamovich, I. V., and Rich, J. W., 'Electron-Beam Generated High Pressure Air Plasma Enhanced by Optical Pumping," AIAA Paper 2001-0346, 2001.

8. Lai, F. C., "Effects of Buoyancy on Electrohydrodynamic-Enhanced Forced Convection in a Horizontal Channel," *Journal of Thermophysics and Heat Transfer*, Vol. 12, No. 3, pp. 431-436.

9. Yabe, A., Mori, Y., and Hijikata, K., "EHD Study of the Corona Wind Between Wire and Plate Electrodes," *AIAA Journal*, Vol. 16, No. 4, 1978, pp. 340-345.

10. von Engel, A., *Ionized Gases*, Oxford at the Clarendon Press, London, 1955, pp. 224-227.

11. Aubrecht, L., Stanek, Z., and Koller, J., "Corona Discharge on Coniferous Trees-Spruce and Pine," *Europhysics Letters*, Vol. 53, No. 3, 2001, pp. 304-309.

12. Hill, J. W., Feigl, D. M., and Baum, S. J., *An Introduction to General Organic, and Biological Chemistry*, 4th ed., Macmillan Pub. Co., 1993, p. 293.

13. Lifshitz, A., "Ignition Delay Times," in *Handbook of Shock Waves*, Vol. 3, ed. by A. Lifshitz, Academic Press, New York, 2001, p. 239.

14. Lee, J. H. S., "Detonation Waves in Gaseous Explosives," in *Handbook of Shock Waves*, Vol. 3, ed. by A. Lifshitz, Academic Press, New York, 2001, p. 344.

15. Yano, R., Contini, V., Plonjes, E., Palm, P., Merriman, S., Aithal, S., Adamovich, I., Lempert, W., Subramanian, V., and Rich, J. W., "Supersonic Nonequilibrium Plasma Wind-Tunnel Measurements of Shock Modification and Flow Visualization," *AIAA Journal*, Vol. 38, No. 10, 2000, pp. 1879-1888.

16. Ershov, A., Ardelyan, N., Chuvashev, S., Shibkov, V., and Timofeev, L., "Probe Diagnostics of Gas Discharges in Supersonic Airflows," *AIAA Journal*, Vol. 39, No. 11, 2001, pp. 2180-2187.

17. Leonov, S., Bityurin, V., and Kolesnichenko, Y., "Dynamic of a Single-Electrode HF Filament in Supersonic Airflow," AIAA Paper 2001-0493, 2001.

18. Menart, J., Shang, J., and Hayes, J., "Development of a Langmuir Probe for Plasma Diagnostic Work in High Speed Flow," AIAA Paper 2001-2804, 2001.

19. Deaconu, S., Coleman, H. W., and Wu, S. T., "Plasma Study on Ionization of Flowing Gases by Direct Current Electric Discharge," *AIAA Journal*, Vol. 41, No. 4, 2003, pp. 633-640.

20. Emanuel, G., *Analytical Fluid Dynamics*, 2nd ed.. CRC Press, Boca Raton, Fl., Sec. 12.2. 2001.

21. Emanuel, G., Satyanand, U. S., and Lu, F. K., "Performance of a Shock Tube with a Large Area Contraction," accepted for publication, *AIAA Journal*, 2005.

22. Salas, M. D., "Shock Wave Interaction with an Abrupt Area Change," NASA, T. P. 3113, 1991.

23. Stussey, W. S., Liu, H. C., Lu, F. K., and Wilson, D. R., "Detonation Wave Driver for Enhancing Shock Tube Performance," AIAA Paper 96-2195, 1996.

24. Anderson, J. D., "Fundamentals of Aerodynamics," 2nd ed., McGraw-Hill Inc., NY, 1991, Sec. 9.2, pp. 460-477.

25. Deaconu, S., Coleman, H. W., and Wu, S. T., "Experimental Study of the Ionization of Flowing Gases by DC Corona Discharge," AIAA Paper 2001-2943, 2001.

26. "Crystallinity," http://www.dupont.com/teflon/films.

27. Holman, J. P., *Experimental Methods for Engineers*, 6th ed., McGraw-Hill Inc., NY, 1994, Sec. 3.4, pp. 49-50.

28. Teare, J. D., "Ionization behind Shock Waves," *Ionization in High Temperature Gases*, ed. by K. E. Shuler, Academic Press, NY, Vol. 12, 1963, pp. 217-283.

29. Lin, S. C., Neal, R. A., and Fyfe, W. I., "Rate of Ionization behind Shock Waves in Air. I. Experimental Results," *Physics of Fluids*, Vol. 5, 1962, pp. 1633-1648.

30. Lin, S. C. and Teare, J. D., "Rate of Ionization behind Shock Waves in Air. II. Theoretical Interpretation," *Physics of Fluids*, Vol. 6, 1963, pp. 355-374.

BIOGRAPHICAL STATEMENT

The author was born in Mangalore, a town in southern part of India in 1941. He got his school education in Bangalore, capital of Karnataka State, India. He received Bachelor of Mechanical Engineering degree from University of Mysore, Karnataka State, India, in 1963. He received Master of Engineering in Design of Process Machines (Pumps and Compressors) from the Regional College, Allahabad, India, in 1970. He served from 1964 to 2000 in various capacities as Lecturer, Assistant Professor and Professor of Mechanical Engineering in Regional College, Suratkal, Mangalore, India and in Bangalore Institute of Technology, Bangalore, India and retired in 2000. He then enrolled in Spring 2001 as a PhD student in Aerospace Engineering at University of Texas at Arlington, Arlington, Tx, USA and successfully completed the program in 2005.